Space Sci Rev
DOI 10.1007/s11214-014-0038-6

Magnetic Helicity and Large Scale Magnetic Fields: A Primer

Eric G. Blackman

Received: 13 January 2014 / Accepted: 4 February 2014

Abstract Magnetic fields of laboratory, planetary, stellar, and galactic plasmas commonly exhibit significant order on large temporal or spatial scales compared to the otherwise random motions within the hosting system. Such ordered fields can be measured in the case of planets, stars, and galaxies, or inferred indirectly by the action of their dynamical influence, such as jets. Whether large scale fields are amplified in situ or a remnant from previous stages of an object's history is often debated for objects without a definitive magnetic activity cycle. Magnetic helicity, a measure of twist and linkage of magnetic field lines, is a unifying tool for understanding large scale field evolution for both mechanisms of origin. Its importance stems from its two basic properties: (1) magnetic helicity is typically better conserved than magnetic energy; and (2) the magnetic energy associated with a fixed amount of magnetic helicity is minimized when the system relaxes this helical structure to the largest scale available. Here I discuss how magnetic helicity has come to help us understand the saturation of and sustenance of large scale dynamos, the need for either local or global helicity fluxes to avoid dynamo quenching, and the associated observational consequences. I also discuss how magnetic helicity acts as a hindrance to turbulent diffusion of large scale fields, and thus a helper for fossil remnant large scale field origin models in some contexts. I briefly discuss the connection between large scale fields and accretion disk theory as well. The goal here is to provide a conceptual primer to help the reader efficiently penetrate the literature.

Keywords Magnetic fields · Galaxies: Jets · Stars: Magnetic field · Dynamo · Accretion · Accretion disks · Cosmology: Miscellaneous

1 Introduction

Planets, stars, galaxies are all examples of astrophysical rotators that reveal direct or indirect evidence for large scale ordered magnetic fields (Schrijver and Zwaan 2000; Brandenburg and Subramanian 2005; Shukurov 2005; Beck 2012; Roberts and King 2013). Here "large"

E.G. Blackman (✉)
Department of Physics and Astronomy, University of Rochester, Rochester, NY 14618, USA
e-mail: blackman@pas.rochester.edu

Published online: 16 April 2014

Influence of Rotation & Large Scale B-Fields:

	~25-30 YEARS AGO	TODAY
planetary nebulae (and pPNe)	-quasi-spherical/elliptical -fate of all low mass stars; -interacting fast+slow outflows with inertial channeling	-aspherical/multi-polar -fate of <50% (?) of low mass stars,often very collimated
young stellar objects	bipolar jets ?	bipolar jets !
active galactic nuclei	many produce jets	many produce jets
gamma-ray bursts	spherical explosions? (distance unknown)	long: jets from massive stars? short: jets from NS-NS mergers?
supernovae (?)	spherical explosions	aspherical

Fig. 1 Chart highlighting an emerging realization in astrophysics that more sources originally perceived as spherical may in fact be bipolar, and thus harborers of large scale magnetic field mediated jets

scale implies a coherent flux on scales comparable to the size of the hosting rotator and most importantly, larger than the scale of fluctuations associated with chaotic turbulent flows. In fact, all of these systems show evidence for both small and large scale magnetic fields, so the fact that large scale order persists even amidst a high degree of smaller scale disorder is a core challenge of explaining the emergence of large scale magnetic structures across such disparate classes of rotators.

Large scale magnetic fields are also likely fundamental to coronae and jets from accretion engines around young and dying stars and compact objects (e.g. Blandford and Payne 1982; Konigl 1989; Field and Rogers 1993; Blackman et al. 2001; Blackman and Pessah 2009; Lynden-Bell 2006; Pudritz et al. 2012; Penna et al. 2013). Accreting systems typically exhibit a continuum spectrum and luminosity best explained by matter accreting onto a central object falling deeper into a potential well and thereby releasing positive kinetic energy in the form of radiation or jet outflows. In fact, as Fig. 1 shows, the classes of objects likely harboring jets has increased as observations have improved, and jets likely indicate the role of large scale magnetic fields.

In young stars, pre-planetary nebulae, micro quasars, and active galactic nuclei the jets typically have too much collimated momenta to be driven by mechanisms that do not involve large scale magnetic fields (Bujarrabal et al. 2001; Pudritz et al. 2012). From the jets of AGN, Faraday rotation from ordered helical magnetic fields is directly observed (Gabuzda et al. 2008, 2012; Asada et al. 2008). Because jets are anchored in the accretion engines, they play a role in extracting the angular momentum that allows remaining disc material to accrete. The ionization fractions of accretion disks are commonly high enough, at least in regions near the very center, to be unstable to the magneto-rotational instability (MRI) (Balbus and Hawley 1991, 1998; Balbus 2003). A plethora of numerical simulations now commonly reveal that the systems evolve to a nonlinear turbulent steady state whose Maxwell stress dominates the Reynolds stress and for which large scale ordered magnetic fields emerge with cycle periods ~ 10 orbit periods (e.g. Brandenburg et al. 1995; Davis et al. 2010; Simon et al. 2011; Guan and Gammie 2011; Sorathia et al. 2012; Suzuki and Inutsuka 2013). With the caveat that angular momentum plays a comparatively

subdominant role in structural support for stars, the coronae of stars and the emergence of large scale ordered fields that thread coronal holes of the sun (e.g. Schrijver and Zwaan 2000) can help shed light on related phenomena of the rising and opening up of large scale fields that form jets and coronae from accretion disks.

There are three possibilities for the origin of large scale fields in astrophysical rotators: The first is that the contemporary field is simply the result of advection and compression of the field that was present in the object before it was formed (e.g. Braithwaite and Spruit 2004; Kulsrud et al. 1997; Lovelace et al. 2009; Subramanian 2010; Widrow et al. 2012). The second is that the field is in fact dynamo produced in situ, extracting free energy from shear, rotation and turbulence in such a way as to sustain the field against turbulent diffusion (e.g. Moffatt 1978; Parker 1979; Ruzmaikin et al. 1988; Shukurov 2005; Charbonneau 2013). The third possibility is some combination of the two (e.g. Kulsrud and Zweibel 2008). In systems like the Sun and Earth where cycle periods involving field reversals are observed, the need for in situ dynamo amplification is unambiguous. For galaxies or accretion disks, the evidence for in situ amplification of large scale fields is more indirect. Regardless of whether the fields are initially frozen in and advected, amplified in situ, or a combination of the two, the evolution of magnetic helicity is very helpful for understanding the physics of magnetic field origin as we shall see.

Much of what we can observationally infer about magnetic fields of planets, stars, and accretion disks comes from information external to where the real action of magnetic field amplification and conversion of kinetic to magnetic energy occurs. Yet, most theory and simulation of astrophysical dynamos focuses on the interiors. This situation contrasts that of our own galaxy where we observe the field from within (e.g. Van Eck et al. 2011; Beck 2012), albeit on time scales too short to observe its dynamical evolution. A related point is that the hidden interiors of astrophysical rotators are typically flow dominated, with the magnetic field energy density generally weaker than that of the kinetic energy. However in the surrounding coronae of stars, accretion disks (and maybe even for galaxies) the field dominates the kinetic energy. Thus we must learn about the flow-dominated interiors from observations of the magnetically dominated exteriors and understand the coupling between the two. Laboratory plasmas of fusion devices are in fact magnetically dominated and there are many lessons learned from this context. Tracking magnetic helicity evolution has proven helpful for understanding the field evolution in both magnetically dominated and flow dominated circumstances.

In this paper I discuss basic principles of magnetic helicity evolution to guide the physical intuition of how large scale magnetic fields arise and evolve. This overview represents one path through the subject and is intended as a conceptual primer to ease immersion in the literature rather than a complete detailed review. Many relevant papers will therefore regrettably go uncited—a situation that I find increasingly difficult to avoid. A example of an earlier more detailed review is Brandenburg and Subramanian (2005).

In Sect. 2, I discuss the key physical properties of magnetic helicity that are central to all subsequent topics discussed. In Sect. 3, I summarize the conceptual progress of how these principles apply to modern developments in magnetic dynamo theory. In Sect. 4, I describe the simple two-scale model for closed systems that has come to be useful for gaining unified insight of large scale field evolution and dynamo saturation more quantitatively. I discuss several applications of the two-scale theory: dynamo saturation, the resilience of helical fields to turbulent diffusion, and dynamical relaxation. In Sect. 5, I discuss the role of helicity fluxes and their relation to the results Sect. 4. In Sect. 6, I briefly discuss the issue of gauge non-invariance of magnetic helicity. I conclude in Sect. 7, emphasizing the expectation that both signs of magnetic helicity on different scales should appear in astrophysical rotators

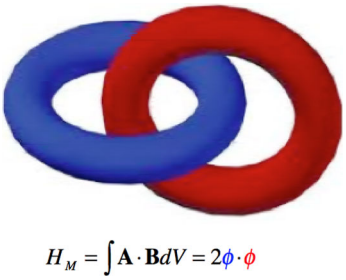

Fig. 2 Magnetic helicity of two linked flux equals twice the product of their magnetic fluxes

with coronal cycle periods, and comment on the connections between magnetic helicity dynamics and accretion disk theory.

2 Key Properties of Magnetic Helicity

Here I introduce some basic properties of magnetic helicity that underlie its role in large scale field generation and are essential for the sections that follow.

2.1 Magnetic Helicity as a Measure of Magnetic Flux Linkage, Twist, or Writhe

Magnetic helicity is defined as volume integral of the dot product of vector potential $\mathbf{A}$ and magnetic field $\mathbf{B} = \nabla \times \mathbf{A}$, namely

$$\int \mathbf{A} \cdot \mathbf{B} dV. \tag{1}$$

To see why this is a measure of magnetic linkage (e.g. Moffatt 1978; Berger and Field 1984), consider two thin linked magnetic flux tubes as shown in Fig. 2, with cross sectional area vectors $d\mathbf{S}_1$ and $d\mathbf{S}_2$ respectively. Let $\Phi_1 = \int \mathbf{B}_1 \cdot d\mathbf{S}_1$ be the magnetic flux in tube 1, where $\mathbf{B}_1$ is the magnetic field. Similarly, for flux tube 2 we have $\Phi_2 = \int \mathbf{B}_2 \cdot d\mathbf{S}_2$ where $\mathbf{B}_2$ is the magnetic field. For both tubes, we assume that the fields are of constant magnitude and parallel to $d\mathbf{S}_1$ and $d\mathbf{S}_2$ respectively. The volume integral of Eq. (1) contributes only where there is magnetic flux. Thus we can split the magnetic helicity into contributions from the two flux tube volumes to obtain

$$\int \mathbf{A} \cdot \mathbf{B} dV = \iint \mathbf{A}_1 \cdot \mathbf{B}_1 dl_1 dS_1 + \iint \mathbf{A}_2 \cdot \mathbf{B}_2 dl_2 dS_2, \tag{2}$$

where we have factored the volume integrals into products of line and surface integrals, with the line integrals taken along the direction parallel to $\mathbf{B}_1$ and $\mathbf{B}_2$. Since the magnitudes of $\mathbf{B}_1$ and $\mathbf{B}_2$ are constant in the tube, we can pull $\mathbf{B}_1$ and $\mathbf{B}_2$ out of each of the two line integrals on the right of Eq. (2) to write

$$\int \mathbf{A} \cdot \mathbf{B} dV = \int A_1 dl_1 \int B_1 dS_1 + \int A_2 dl_2 \int B_2 dS_2 = \Phi_2 \Phi_1 + \Phi_1 \Phi_2 = 2\Phi_1 \Phi_2, \tag{3}$$

where we have used Gauss' theorem to replace $\int A_1 dl_1 = \Phi_2$, the magnetic flux of tube 2 that is linked through tube 1. and similarly $\int A_2 dl_1 = \Phi_1$. Note that if the tubes are not linked, then the line integral would vanish and there would be no magnetic helicity.

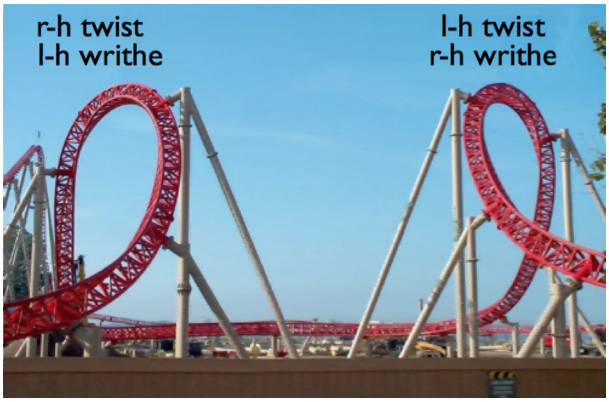

Fig. 3 Picture of a "twisted horseshoe roll" element of a roller coaster at Cedar Point in Sandusky, Ohio, USA. The large scale loops are "writhe" as defined in the text and the rotation of the tracks along the direction of the coaster path is "twist". The *loop on the left* has left-handed writhe and right handed twist. The *loop on the right* has right-handed writhe and left-handed twist. The overall trip on the coaster is a closed path, the rest of which is not shown

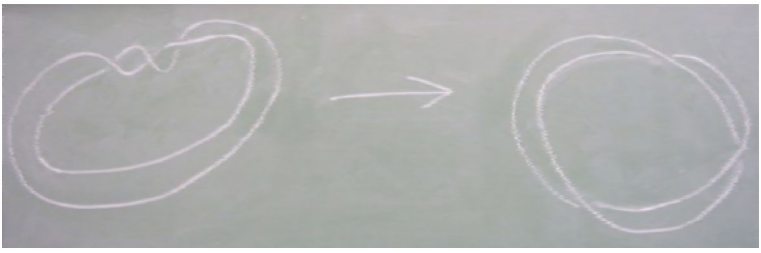

Fig. 4 The sketch illustrates two concepts. The first is magnetic relaxation: The small scale twist of the ribbon on the left has relaxed to the largest scale available to it in the *right figure*. The right configuration is a lower energy state for the same magnetic helicity as that in the left. The second concept is that these structures can also be viewed as two strands, so that one can qualitatively appreciate some equivalence between twist of a ribbon and linkage of a pair of strands. In the text, this is made more quantitative for a different example shown in Fig. 5

Having established that the magnetic helicity measures linkage, we are poised to understand how helicity can also be equivalently characterized as a measure of magnetic twist and writhe. Examples of local twist and writhe are seen in Fig. 3, which is a roller coaster element at Cedar Point in Sandusky Ohio (USA). The large loops each correspond to writhe, and twist is measured along the track. (Note that "writhe" here is what Bellan (2000) calls "overlap" and "twist" here is what Bellan (2000) calls "writhe".) A twisted ribbon is also shown in Fig. 4, where the amount of twist is conserved between the two panels but transferred from small to large scales.

Quantitatively relating linkage to twist is nicely accomplished experimentally with strips of paper, a scissors and some tape (e.g. Bellan 2000). This is illustrated in Fig. 5. The two panels show configuations with equivalent amounts of helicity as I now describe. Start with a straight strip of paper (say 20 cm long and 2 cm wide) and give the strip a full right handed twist around its long axis (by holding the bottom with your left and twisting at the top with your right hand). Now fasten the ends so that it is a twisted closed loop. This provides a model for a flattened, twisted closed magnetic flux tube. The result is Fig. 5a. Now consider that this tube could in fact have been composed of two adjacent flattened tubes pressed together side by side. Separating these adjacent tubes is accomplished by use of a scissors. Cut the along the center line of the strip all the way around and the result is two linked ribbons, each of 1/2 the width of the original, and each with one right handed

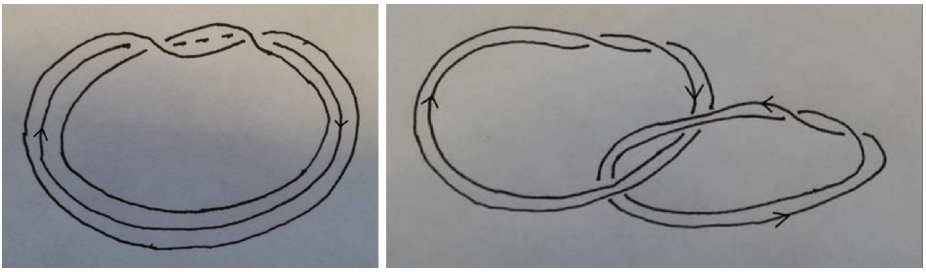

Fig. 5 The two panels show schematics of magnetic ribbon systems with equivalent amounts of magnetic helicity. The *left panel* shows a single twisted ribbon. If this were represented by a strip of paper, cutting along the centerline then results in the *right panel*. The single thick ribbon with one right handed twist has been converted to two linked ribbons of 1/2 half the width of the original, and each with a right handed twist. This figure illustrates why helicity can be represented as twist, linkage, or some combination of the two

twist. The result is shown in Fig. 5b. The use of scissors in this way has not changed the overall helicity of the system, but has transformed it into different forms as follows: If the original unseparated ribbon had a magnetic flux Φ then each of the 1/2 width ribbons have flux $\Phi/2$. From the above discussion of linkage, the linkage of these two new ribbons gives a contribution of helicity $2\Phi^2/4 = \Phi^2/2$. But the original uncut ribbon had a single right handed twist with total flux Φ. For the helicity of the initial twisted ribbon to equal that of the two linked twisted ribbons, any twisted ribbon must contribute a helicity equal to its flux squared. Thus helicity is thus conserved as follows: Φ^2 is the helicity associated with the initial twisted ribbon, and this is then equal to the sum of helicity from the linkage of the two half-thickness flux tubes $\Phi^2/2$, plus that from the right handed twists in each of these two half- thickness ribbons $2 \times (\Phi/2)^2 = \Phi^2/2$. This conveys how both linkage and twist are manifestations of magnetic helicity.

To see the relation between twist and writhe, consider again a straight paper ribbon. As above, give the ribbon one right handed twist around its long axis holding the other end fixed as in Fig. 6a. Imagine that the ends A and B are identified as the same location so it is really a closed twisted loop. Now push the ends A and B inward toward each other and the ribbon will buckle, as seen in Fig. 6b. A side view of this buckling is shown in Fig. 6c. If the ends A and B are identified, then the result is now a loop with a single unit of writhe—a large scale loop through which you can thread a rigid pole—that was derived from a single unit of twist. Thus one unit of twist helicity is equivalent to one unit of writhe helicity.

In short, one unit of twist helicity for a tube or ribbon of magnetic flux Φ is equal to one unit of writhe helicity for the same flux tube, and both are separately equal to 1/2 of the helicity resulting from the linkage of two untwisted flux tubes of flux Φ. These three different, but equivalent ways of thinking about magnetic helicity are instructive for extracting the physical ideas in what follows.

2.2 Evolution of Magnetic Helicity

The time evolution equation for magnetic is simply derived in magnetohydrodynamics: The electric field is given by

$$\mathbf{E} = -\nabla\Phi - \frac{1}{c}\partial_t \mathbf{A}, \tag{4}$$

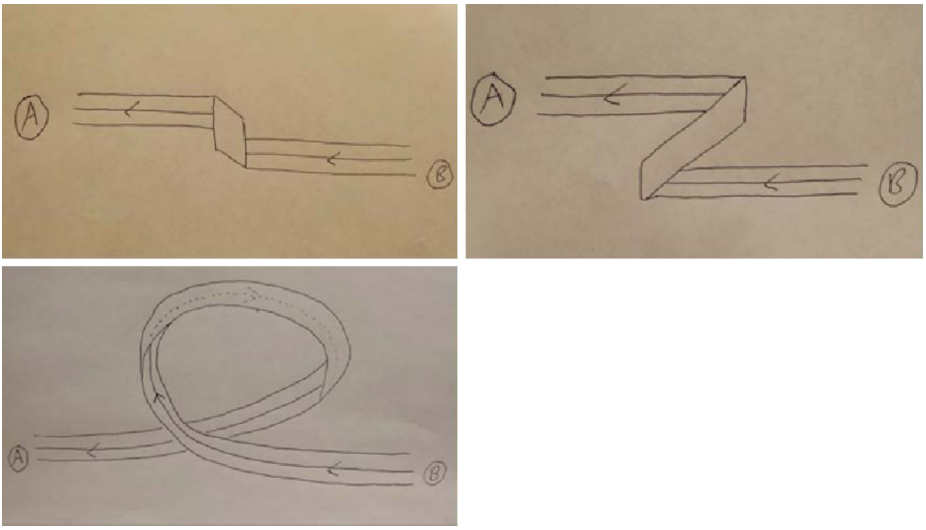

Fig. 6 The *three panels* show how to transform twist helicity into writhe helicity. (*Top left*) Start with a straight flat ribbon with one unit of right handed twist. One could imagine that the ends A and B are identified with each other and so it is a mathematically a closed ribbon loop with a twist. (*Top right*) Push the ends A and B toward each other until the ribbon buckles upward. (*Bottom*) A side view shows the writhe. The result is a writhed, closed loop

where Φ and $\mathbf{A}$ are the scalar and vector potentials. Using $\mathbf{B}\cdot\partial_t\mathbf{A} = \partial_t(\mathbf{A}\cdot\mathbf{B}) + c\mathbf{E}\cdot\mathbf{B} - c\nabla\cdot(\mathbf{A}\times\mathbf{E})$, where the latter two terms result from Maxwell's equation

$$\partial_t\mathbf{B} = -c\nabla\times\mathbf{E} \tag{5}$$

and the identity $\mathbf{A}\cdot\nabla\times\mathbf{E} = \mathbf{E}\cdot\mathbf{B} - \nabla\cdot(\mathbf{A}\times\mathbf{E})$, we take the dot product of Eq. (4) with $\mathbf{B}$ to obtain the evolution of the magnetic helicity density

$$\partial_t(\mathbf{A}\cdot\mathbf{B}) = -2c\mathbf{E}\cdot\mathbf{B} - \nabla\cdot(c\Phi\mathbf{B} + c\mathbf{E}\times\mathbf{A}). \tag{6}$$

If we average this equation over a simply connected volume that has no boundary terms, the last terms would not contribute and we obtain

$$\partial_t\langle\mathbf{A}\cdot\mathbf{B}\rangle = -2c\langle\mathbf{E}\cdot\mathbf{B}\rangle. \tag{7}$$

In MHD Ohm's law is

$$\mathbf{E} = -\mathbf{v}\times\mathbf{B}/c + \eta\mathbf{J}, \tag{8}$$

where $\mathbf{V}$ is the flow velocity and $\eta = 4\pi\nu_M/c^2$ is the resistivity for a magnetic diffusivity ν_M. For ideal MHD ($\eta = 0$) the right hand side of (7) is zero, highlighting the conservation of magnetic helicity density (and thus magnetic helicity) for a closed volume under ideal conditions and independent of the presence of velocity flows.

For comparison, the magnetic energy density evolution, obtained by dotting Eq. (5) with $\mathbf{B}$ and using Eq. (8) is given by

$$\frac{1}{8\pi}\partial_t\langle\mathbf{B}^2\rangle = -\eta\langle\mathbf{J}^2\rangle - \frac{1}{c}\langle\mathbf{v}\cdot(\mathbf{J}\times\mathbf{B})\rangle, \tag{9}$$

where $\mathbf{J}\equiv\frac{c}{4\pi}\nabla\times\mathbf{B}$.

2.3 Magnetic Helicity is Typically Better Conserved than Magnetic Energy

In the absence of dissipation, magnetic helicity is exactly conserved in MHD for a closed system but magnetic energy can be exchanged with a velocity field. If we ignore the latter, when the ratio of time scale for resistive decay of magnetic energy to that of magnetic helicity is small, magnetic helicity is more strongly conserved than magnetic energy. To demonstrate when this is true, we must consider that a typical astrophysical system is often turbulent, so there is not just one scale of the field but a spectrum. The question becomes for what spectra of magnetic energy and magnetic helicity does the latter decay more slowly than the former? Following Blackman (2004) and working in the Coulomb gauge, we write the (statistically or volume) averaged magnetic energy density as

$$\left\langle \mathbf{B}^2 \right\rangle / 8\pi = M = \int_{k_0}^{k_{\nu_M}} M_k dk, \tag{10}$$

where the brackets indicate an average, k_0 and k_{ν_M} are the minimum and maximum (resistive) wave numbers, and the one-dimensional magnetic energy density spectrum is given by

$$M_k \equiv \frac{1}{8\pi} \int |\tilde{\mathbf{B}}|^2 k^2 d\Omega_k = \int |\tilde{\mathbf{A}}|^2 k^4 d\Omega_k \propto k^{-q}. \tag{11}$$

Here Ω_k is the solid angle in wave-number space, q is an assumed constant, and the tilde indicate Fourier transforms. The magnetic helicity density spectrum is then

$$\begin{aligned} H_k &\equiv \frac{1}{16\pi} \int \left[\tilde{\mathbf{A}}(k) \tilde{\mathbf{B}}^*(k) + \tilde{\mathbf{A}}^*(k) \tilde{\mathbf{B}}(k) \right] k^2 d\Omega_k \\ &= M_k f(k)/k, \end{aligned} \tag{12}$$

where * indicates complex conjugate and $f(k) \propto k^{-s}$ is used to define the fraction of magnetic energy that is helical at each wave number and s is taken as a constant. We then also have correspondingly

$$\langle \mathbf{A} \cdot \mathbf{B} \rangle = \int_{k_0}^{k_{\nu_M}} f(k) M_k k^{-1} dk, \tag{13}$$

and the current helicity density

$$\langle \mathbf{J} \cdot \mathbf{B} \rangle = \int_{k_0}^{k_{\nu_M}} f(k) k M_k dk. \tag{14}$$

Now, using Eq. (7) for a closed system we have

$$8\pi \, \partial_t H = \partial_t \langle \mathbf{A} \cdot \mathbf{B} \rangle = -2\nu_M \langle \mathbf{J} \cdot \mathbf{B} \rangle, \tag{15}$$

and Eq. (9) gives in the absence of velocity flows,

$$8\pi \, \partial_t M = \partial_t \left\langle \mathbf{B}^2 \right\rangle = -2\nu_M \left\langle (\nabla \mathbf{B})^2 \right\rangle. \tag{16}$$

Then combining (13)–(16), we then obtain

$$\tau_H = \frac{-H}{\partial_t H} = \frac{\int_{k_L}^{k_{\nu_M}} f(k) M_k k^{-1} dk}{2\nu_M \int_{k_L}^{k_{\nu_M}} f(k) k M_k dk} \tag{17}$$

and

$$\tau_M = \frac{-M}{(\partial_t M)_{res}} = \frac{\int_{k_L}^{k_{\nu_M}} M_k dk}{2\nu_M \int_{k_L}^{k_{\nu_M}} k^2 M_k dk}, \tag{18}$$

for the time scales of magnetic helicity and magnetic energy decay respectively. The subscript "*res*" indicates the contribution from the penultimate term in (16) only. The range of s and q for which $R \equiv \frac{\tau_H}{\tau_M} > 1$ corresponds to regime in which the magnetic helicity decays more slowly than the magnetic energy. Blackman (2004) showed that $R > 1$ for the combination of $s > 0$ and $3 > q > 0$ and that $R < 1$ for small $0 < q < 1$ and $s < 0$. The latter range would correspond to a very unusual circumstance in which all the magnetic helicity were piled up at small scales. Most commonly therefore, the range for which $R > 1$ applies and magnetic helicity is typically better conserved than magnetic energy.

2.4 Minimum Energy State of Helical Magnetic Fields

The conclusion of the previous section—that magnetic helicity usually decays more slowly than magnetic energy—justifies *a posteriori* the relevance of the question that Woltjer (1958a) considered: If the magnetic helicity is conserved for a magnetically dominated system (ignoring velocities), what magnetic field configuration minimizes the energy? Using a variational principle calculation, Woltjer (1958a) found that the answer is a configuration for which $\mathbf{J} = \frac{c}{4\pi}\nabla\times\mathbf{B} = f(\mathbf{x})\mathbf{B}$, where $f(\mathbf{x})$ is a scalar function that must therefore satisfy $\mathbf{B}\cdot\nabla f = 0$. Taylor (1974, 1986) considered the same question but assumed that magnetic helicity is approximately conserved when averaged over sufficiently large scales even in the presence of a small but finite resistive dissipation. Essentially, f becomes a measure of the inverse gradient scale of the helical magnetic field and so minimizing the energy means decreasing f as much as possible. The small amount of dissipation aids this relaxation via small scale reconnection as needed, such that the overall relaxed state of the field is one in which the small scale gradients smooth out to allow the gradient scales to reach the largest possible subject to the boundary conditions. This, in turn, uniquely determines f as a function of the specific boundary conditions. (Figure 4 shows a simple helicity conserving relaxation process where reconnection is not actually needed.) The arguments of Woltjer (1958a) and Taylor (1974) essentially assumed that $R > 1$. The previous section shows the specific spectral conditions for this to be viable, and solidifies the assumptions on which these results were based.

That Woltjer (1958a) arrived at a force-free, minimum energy state under the conditions imposed—no velocity flows, no dissipation, and a closed volume—is evident even without a variational calculation. Imagine a system with initially no pressure gradients and no velocity with a field configuration that is not force free, i.e., $\mathbf{J}\times\mathbf{B} \neq 0$. A velocity flow will swiftly develop, violating the assumption that there is no velocity. The only way that the velocity (and thus kinetic energy) could remain zero is if the field produces no acceleration, i.e. is force free. The assumption of no velocity is therefore enough to conclude that the field must be force-free in a steady state. Moreover, in a closed system, a force free field is fully helical, namely $\langle\mathbf{J}\cdot\mathbf{B}\rangle = -\langle\mathbf{B}\cdot\nabla^2\mathbf{A}\rangle$, so that the 1-D Fourier spectrum of current helicity $H_c(k)$ would be $k^2 H_M(k)$ where $H_M(k)$ is the magnetic helicity spectrum. For a fully helical system, $kH_M(k) = M(k) = H_c(k)/k$. Suppose the magnetic energy is predominately at a single wavenumber k_E, and we ask whether k_E must increase or decrease to minimize the magnetic energy: If magnetic helicity is conserved then $k_E H_M(k_E) = M(k_E)$ would remain constant as k_E changes. The magnetic energy $k_E M(k_E)$ thus decreases with decreasing k_E.

As a result, minimizing the magnetic energy for a fixed magnetic helicity would lead to as small of a k as possible. This is the essence of the "Taylor relaxed" state.

Note also that if we drop the assumption that there is no velocity flow, then the momentum equation for incompressible ($\nabla \cdot \mathbf{v} = 0$, $\rho =$ constant) flow in the absence of microphysical dissipation is

$$\frac{\partial \mathbf{v}}{\partial t} = \rho \mathbf{v} \times (\nabla \times \mathbf{v}) - \nabla\left(\mathbf{v}^2/2 + \frac{P}{\rho}\right) + \frac{\mathbf{J} \times \mathbf{B}}{\rho}. \tag{19}$$

Dotting with $\mathbf{v}$ and averaging over a closed volume gives

$$\left\langle \partial \mathbf{v}^2/\partial t \right\rangle = \left\langle \mathbf{v} \cdot (\mathbf{J} \times \mathbf{B}) \right\rangle. \tag{20}$$

In the absence of dissipation, the right hand side of Eq. (20) is also the only contributing term to the evolution of magnetic energy in Eq. (9). Thus $\langle \mathbf{v} \cdot (\mathbf{J} \times \mathbf{B}) \rangle = 0$ is the generalization to the force free state when velocities are allowed, for it is the only way for both the magnetic and kinetic energies to remain steady. Woltjer (1958b) extended Woltjer (1958a) by deriving integrals of the motion for more general hydromagnetic flows and Field (1986) focused on a static extension of Woltjer (1958a) to include pressure gradients. However, the derivation of Eq. (20) above provides a simple articulation of the generalization to the force free condition when velocity flows are allowed.

This subsection has focused on the steady state, not the dynamical relaxation to that state. In fact, magnetic relaxation is a time dependent. Even in the magnetically dominated regime of astrophysical coronae and laboratory fusion plasmas where magnetic relaxation is considered (e.g. Bellan 2000; Ji and Prager 2002); this relaxation is in fact a large scale dynamo (LSD), because large scale helical fields grow where none were present initially, and as a consequence of helical (magnetic) energy input on small scales. In the discussion of dynamos in the next sections, I will discuss how this relaxation and the more traditional flow driven large scale field growth are different flavors within a unified framework. Magnetic helicity evolution is fundamental to both.

3 Helicity and Large Scale Dynamo Saturation: Conceptual Progress

3.1 Types of Dynamos and Approaches to Study Them

Dynamos describe the growth or sustenance of magnetic fields against the otherwise competing exponential decay. They can be divided into two major classes:

Small Scale Dynamo (SSD): This corresponds to magnetic energy amplification by turbulent velocity flows for which the dominant magnetic energy growth occurs primarily at and below the velocity forcing scale (e.g. Kazanstev 1968; Schekochihin et al. 2002; Bhat and Subramanian 2013; Brandenburg and Lazarian 2013). There is a large body of work addressing the overall magnetic energy spectra of such small scale dynamos when the system is isotropically forced without kinetic helicity. We will not focus on small scale dynamos in what follows.

Large Scale Dynamo (LSD): For LSDs, the magnetic energy grows on spatial or temporal scales larger than the dominant input scale. The input energy can take different forms but in all cases, the fact that the field grows on scales large compared to those of the input energy always requires a large scale electromotive force (EMF) aligned with the large scale

or mean magnetic field, such that $(\overline{\mathbf{v} \times \mathbf{b}}) \cdot \overline{\mathbf{B}} \neq 0$, where the overbars indicate a spatial, temporal, or ensemble average and $\mathbf{v}$ and $\mathbf{b}$ are the velocity magnetic fields associated with turbulent fluctuations when the total velocity and magnetic field are written as sums of fluctuations plus mean values as $\mathbf{V} = \mathbf{v} + \overline{\mathbf{B}}$ and $\mathbf{B} = \mathbf{b} + \overline{\mathbf{B}}$ respectively. This implies a source of large scale magnetic helicity is involved in field amplification as we shall see more explicitly later.

Two sub-classes of LSDs can be distinguished, based on the nature of the dominant energy input:

1. *Flow Dominated*: For this subclass, the input energy is kinetic energy dominated and the EMF can be sustained, for example, by kinetic helicity, as in the classic Parker-type solar dynamo and its extensions (e.g. Moffatt 1978; Parker 1979; Krause and Rädler 1980; Pouquet et al. 1976; Blackman and Field 2002 and Blackman and Brandenburg 2002). Alternatively, there is emerging agreement that a combination of shear and fluctuating kinetic helicity can conspire to produce an LSD (Vishniac and Brandenburg 1997; Brandenburg 2005; Yousef et al. 2008; Heinemann et al. 2011; Mitra and Brandenburg 2012; Sridhar and Singh 2013). The EMF can also be sustained by magnetic helicity fluxes, either local (within sectors of a closed volume) or global (fluxes thought the system boundary) as we will later discuss.

2. *Magnetic Relaxation LSD*: This subclass of LSDs occurs when a system is initially magnetic energy dominated and the EMF is sustained by magnetically dominated quantities. Typically, injection of small scale magnetic helicity drives instabilities that facilitate the relaxation of the system and transfer of the magnetic helicity to large scales. It is a dynamo because field grows on large scales where there was little initially, and the field on large scales is sustained against decay. In plasma fusion devices where such MRD occur, helicity fluxes are the key sustainer of the EMF (e.g. Strauss 1985, 1986; Bhattacharjee and Hameiri 1986; Ortolani and Schnack 1993; Ji et al. 1995; Bellan 2000; Ji and Prager 2002). In astrophysics such MR-LSDs likely occur in coronae, where the field is injected from below on small scales relative to the corona and further relaxation occurs. Astrophysical rotators with coronae likely have flow driven dynamos in the interior, coupled to MRDs in coronae. Ironically, for the sun and stars, the observed field measured is from the base of the corona outward. Thus we can directly observe the MR-LSD processes better than the interior flow driven LSD, although the two are dynamically coupled.

In studying dynamos there are different approaches used depending on the goal. One approach is the "kitchen sink" approach, that is, try to perform quasi-realistic numerical experiments to match observational features with as realistic of conditions as possible given numerical limitations (e.g. Glatzmaier 2002). A second approach is to carry out semi-empirical model calculations based on linear theories but with dynamo transport coefficients empirically tuned to match general observational features and cycle periods (e.g. Dikpati and Gilman 2009; Charbonneau 2013), and without going after the physics of nonlinear quenching. A third approach, and the one most reviewed in this primer, is identifying basic principles of EMF sourcing and quenching. This involves pursuit of a "first principles" mean field theory and comparison to minimalist simulations to test the predictions of the theory. The goal is to develop a mean field theory that isolates the key physics from the nonlinear mess and eventually use the insights gained to inform more detailed models.

3.2 20th Century vs. 21st Century Dynamos: Physical Role of Magnetic Helicity Conservation

The 20th century textbook mean field dynamo theory (MFDT) of standard textbooks (Moffatt 1978; Parker 1979; Krause and Rädler 1980) is a practical approach to modeling LSDs

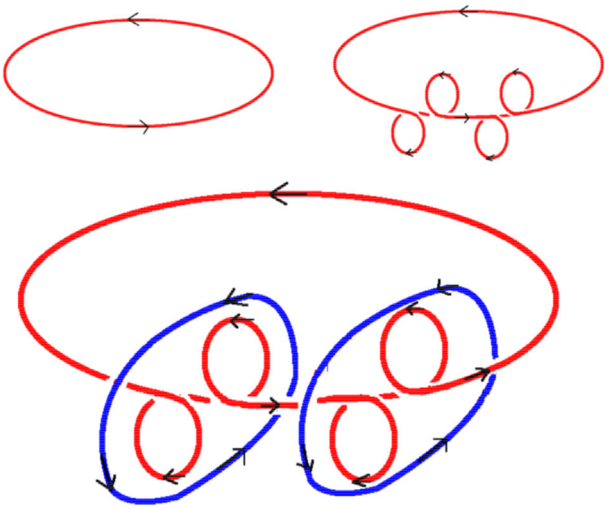

Fig. 7 Two-stage schematic for magnetic field structure in an α^2 dynamo driven by negative kinetic helicity in the conventional 20th century approach with the magnetic field represented as *lines*. The *top right panel* shows a large untwisted toroidal magnetic field ribbon. The *top right panel* shows the action of kinetic helicity on the initial ribbon. The small scale negative kinetic helicity produces each the four small scale poloidal loops. Each small loop incurs a writhe (or overlap) of positive (= right-handed) magnetic helicity. The two intermediate scale poloidal loops encircling the small scale loops in the *bottom panel* represent the resultant mean poloidal field averaged separately over each pair of loops. These intermediate scale loops are linked to the initial large scale torioidal loop. Since a single linked pair of ribbons has 2 units of magnetic helicity, we see that the two poloidal loops linking the torioidal loop have a total 4 total units of right handed magnetic helicity. This helicity in the "large scale field" has come from zero initial magnetic helicity and thus cannot be correct for MHD at large R_M which conserves magnetic helicity. The diagram does not account for the missing small scale magnetic helicity of opposite sign (compare to Fig. 8)

in turbulent rotators. These approaches focused mostly on initially globally reflection asymmetric rotators where the EMF is sustained by kinetic helicity. But for ~ 50 years, this theory lacked a saturation theory to predict how strong the large scale fields get before quenching via the back-reaction of the field on the driving flow.

In fact, the inability of the 20th century textbook theories to predict mean field dynamo saturation arises because they fail to conserve magnetic helicity. This is illustrated in a most minimalist way in the diagrammatic representations of Fig. 7 for the so called α^2 dynamo, a dynamo that just depends on small scale helical velocity motions (discussed more quantitatively later). The figure shows that from an initial toroidal loop, the four small scale helical eddies, each with the same sign of kinetic helicity $\mathbf{v} \cdot \nabla \times \mathbf{v}$ make four small poloidal loops as shown. The result is a net toroidal EMF $\overline{\mathcal{E}}_\phi = \langle v_z b_r \rangle$ which has the same sign inside the loops of all the eddies whether they moved up or down. This in turn leads to two net large scale poloidal loops (shown in blue). But recall that magnetic helicity is a measure of linkage. The first panel has only a single red loop, but seemingly evolves to a configuration with the red loop linked to the two blue loops. That is, the mean field has gone from no helicity, to two units of linkage helicity. This lack of helicity conservation highlights an unphysical feature of 20th century LSD theory.

The commonly used schematics and diagrams of more finely tuned and observationally relevant solar dynamo models, such as flux-transport models (Dikpati and Gilman 2009), also do not conserve magnetic helicity for essentially the same reason as in Fig. 7. There is typically a step where the large scale field gains helicity when a poloidal loop emerges

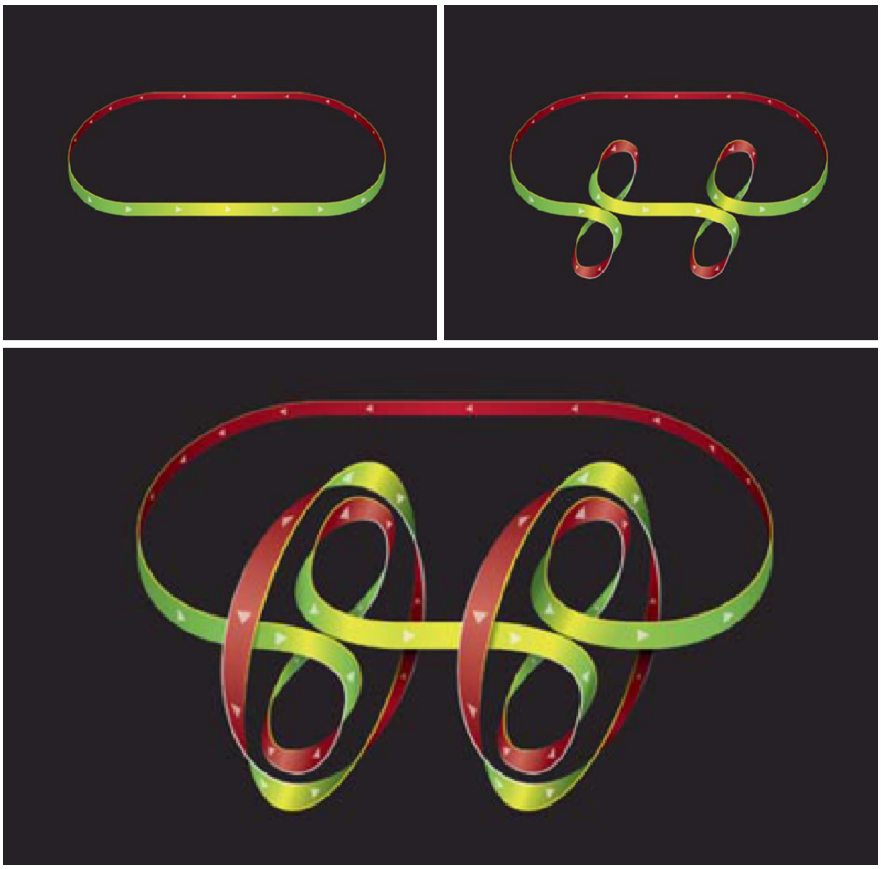

Fig. 8 Modification of Fig. 7 to include magnetic helicity conservation (from Blackman and Hubbard 2014) to include magnetic helicity conservation. The *top left panel* shows a large untwisted toroidal magnetic field ribbon. The *top right panel* shows the action of kinetic helicity on the initial ribbon. The small scale negative kinetic helicity produces each the four small scale poloidal loops. Each small loop incurs a writhe (or overlap) of positive (= right-handed) magnetic helicity. Since magnetic helicity is conserved, each of these four loops also has a negative (= left-handed) twist along the field ribbon. The two intermediate scale poloidal loops encircling the small scale loops in the *bottom panel* represent the resultant mean poloidal field averaged separately over each pair of loops. The intermediate scale poloidal loops have accumulated two units of magnetic twist, one from each of the small loops that they encircle. These intermediate scale loops are also linked to the initial large scale torioidal loop. Since a single linked pair of ribbons has 2 units of magnetic helicity we see that the two poloidal loops linking the torioidal loop have a total 4 total units of right handed magnetic helicity in linkage which exactly balances the sum of $2 + 2$ left handed units of twist on these poloidial loops. In general, the small scale of the twists need not correspond to the same scale as the velocity driving the small scale writhes, though the calculations of Sect. 4 assume such for simplicity

from an initially toroidal field via the action of the Coriolis force. Flux transport dynamos are otherwise impressive in that they can be tuned to agree with large scale observations of the solar magnetic field (e.g. Wang and Sheeley 2003), but the fact that certain parameters must be tuned by hand (rather than derived from first principles) highlights that magnetic helicity dynamics have not yet been incorporated.

How do we reconcile LSDs with the conservation of magnetic helicity? The answer is shown in Fig. 8 (figure from Blackman and Hubbard 2014). There the same set of diagrams

as in Fig. 7 are shown with the field lines represented by ribbons or flux bundles instead of lines. Now conservation of helicity is maintained: the writhe of the loops in the second panel is compensated for by the opposite sign of twist helicity along the loops. The linkage that results in the third panel for the large scale field is compensated for by the exact opposite amount of small scale twist helicity along the loops. This conservation of magnetic helicity of an untwisted loop subjected to writhe can be demonstrated by using an ordinary belt.

The diagrammatic solution to the missing helicity problem is also the key to understanding nonlinear quenching. In a system driven with kinetic helicity, the back reaction on the driving flow comes primarily from the buildup of the small scale twist. Field lines with ever increasing small scale twists become harder to bend. It is this small scale twist that produces a small scale current $\mathbf{j} \equiv \mathbf{J} - \overline{\mathbf{J}}$ (where $\overline{\mathbf{J}} = \nabla \times \overline{\mathbf{B}}$) and a Lorentz force when coupled to the mean field, $\mathbf{j} \times \overline{\mathbf{B}}$, that produces the back reaction against the small scale flow. The driving kinetic helicity acts as a pump, segregating the signs of the magnetic helicity between scales. but the presence of small scale twist eventually quenches which has no dynamo.

How catastrophic this quenching is, depends on the specific type of dynamo: For the α^2 dynamo (a dynamo without differential rotation), the quenching slows the growth to resistively limited rates after an initial fast growth phase, but the field does not decay (Field and Blackman 2002; Blackman and Field 2002). In contrast, for the $\alpha - \Omega$ dynamo (i.e. a dynamo for which the toroidal field growth is dominated by shear from differential rotation), the quenching is such that the field starts to grow and then decays rapidly (e.g. Shukurov et al. 2006; Sur et al. 2007). That helicity fluxes might alleviate quenching and sustain the EMF (e.g. Blackman and Field 2000a; Vishniac and Cho 2001; Brandenburg and Subramanian 2005; Shukurov et al. 2006; Ebrahimi and Bhattacharjee 2014) has emerged as the most plausible way around this decay. Because of the way our understanding of the quenching has developed, the role of magnetic helicity flux is often expressed as a solution to the quenching problem, however the helicity flux could have been the driver of the growth from the start (as in laboratory plasma dynamos, e.g. Strauss 1985, 1986; Bhattacharjee and Hameiri 1986) and thus the issue of quenching would not arise in the discussion in the first place. This is something to keep in mind in reading the literature across subfields.

The physical description described in the previous subsection is supported by detailed calculations. Mathematically coupling the dynamical evolution of magnetic helicity into the dynamo equations can largely explain the saturation seen in simulations. The connection between magnetic helicity and large scale dynamos was first evident in the spectral model of helical MHD turbulence of Pouquet et al. (1976). They demonstrated an inverse transfer growth of large scale magnetic helicity for which the driver is the difference between kinetic and current helicities. In Kleeorin and Ruzmaikin (1982) an equation that couples the small scale magnetic helicity to the mean electromotive force is present, but the time evolution was not studied. The spectral work of Pouquet et al. (1976) was reinterpreted (Field and Blackman 2002) and re-derived (Blackman and Field 2002) as a 'user-friendly' time-dependent mean field theory exemplified for the α^2 dynamo case. Indeed it was found that $\langle \mathbf{v} \cdot \nabla \times \mathbf{v} \rangle$ grows large scale mag. helicity of one sign and small scale mag. helicity of opposite sign. The latter quenches LSD growth and matches simulations of Brandenburg (2001) and subsequent papers. A similar framework shows that large scale helical fields are resilient to turbulent diffusion (Blackman and Subramanian 2013; Bhat et al. 2014) These developments will be discussed later in Sect. 4.

The study of magnetic helicity dynamics in systems unstable to the magneto rotational instability (MRI) is also emerging (e.g. Vishniac 2009; Gressel 2010; Käpylä and Korpi 2011; Ebrahimi and Bhattacharjee 2014): MRI simulations exhibit LSDs driven by an EMF

sustained by something other than kinetic helicity, e.g. current helicity or helicity fluxes. Helicity fluxes may sustain EMF and alleviate premature quenching in realistic systems with global boundaries OR in sub-volume local sectors even if the system is closed (e.g. vertically periodic shearing box). This will be addressed in Sect. 5.

4 Two-Scale Approach to Helicity Dynamics Provides Physical Insight

We now summarize the derivation of the two-scale equations for magnetic helicity evolution from which the above physical discussion arises. We will then discuss two applications of these equations, one for the α^2 dynamo and the second for the resilience of helical fields to decay. A third application to dynamical relaxation is briefly mentioned as well.

4.1 Basic Equations

We follow standard procedures (Blackman and Field 2002; Brandenburg and Subramanian 2005; Blackman and Subramanian 2013) and break each variable into large scale quantities (indicated by an overbar) and fluctuating quantities (indicated by lower case). We indicate global averages by brackets. The overbar indicates a more local average than brackets, (and can also be an average over reduced dimensions) but still over a large enough scale such that both local and global averages of fluctuating quantities vanish.

The analogous procedure that led to Eq. (6) for the evolution of the total magnetic helicity, leads to separate expressions for the contributions to magnetic helicity from the large and small scale given by

$$\frac{1}{2}\partial_t\langle\overline{\mathbf{a}\cdot\mathbf{b}}\rangle = -\langle\overline{\boldsymbol{\mathcal{E}}}\cdot\overline{\mathbf{B}}\rangle - \nu_M\langle\overline{\mathbf{b}\cdot\nabla\times\mathbf{b}}\rangle - \frac{1}{2}\nabla\cdot(c\overline{\phi\mathbf{b}} + c\overline{\mathbf{e}\times\mathbf{a}}), \tag{21}$$

and

$$\frac{1}{2}\partial_t\langle\overline{\mathbf{A}}\cdot\overline{\mathbf{B}}\rangle = \langle\overline{\boldsymbol{\mathcal{E}}}\cdot\overline{\mathbf{B}}\rangle - \nu_M\langle\overline{\mathbf{B}}\cdot\nabla\times\overline{\mathbf{B}}\rangle - \frac{1}{2}\nabla\cdot(c\overline{\Phi}\overline{\mathbf{B}} + c\overline{\mathbf{E}}\times\overline{\mathbf{A}}). \tag{22}$$

where $\overline{\boldsymbol{\mathcal{E}}} \equiv \overline{\mathbf{v}\times\mathbf{b}} = -\overline{\mathbf{E}} + \eta\overline{\mathbf{J}} = -\mathbf{E} + \mathbf{e} + \eta(\mathbf{J}-\mathbf{j})$ is the turbulent electromotive force. The simplest expression for $\overline{\boldsymbol{\mathcal{E}}}$ that connects 20th century dynamo theory to 21st century makes use the 'tau' or 'minimal tau' closure approach for incompressible MHD (Blackman and Field 2002; Brandenburg and Subramanian 2005). This means replacing triple correlations by a damping term on the grounds that the EMF $\overline{\boldsymbol{\mathcal{E}}}$ should decay in the absence of $\overline{B}$. The result is

$$\partial_t\overline{\boldsymbol{\mathcal{E}}} = \overline{\partial_t\mathbf{v}\times\mathbf{b}} + \overline{\mathbf{v}\times\partial_t\mathbf{b}} = \frac{\alpha}{\tau}\overline{\mathbf{B}} - \frac{\beta}{\tau}\nabla\times\overline{\mathbf{B}} - \overline{\boldsymbol{\mathcal{E}}}/\tau, \tag{23}$$

where τ is a damping time and

$$\alpha \equiv \frac{\tau}{3}\left(\frac{\langle\mathbf{b}\cdot\nabla\times\mathbf{b}\rangle}{4\pi\rho} - \langle\mathbf{v}\cdot\nabla\times\mathbf{v}\rangle\right) \quad \text{and} \quad \beta \equiv \frac{\tau}{3}\langle v^2\rangle, \tag{24}$$

and we assume $\langle\mathbf{v}\cdot\nabla\times\mathbf{v}\rangle \simeq \overline{\mathbf{v}\cdot\nabla\times\mathbf{v}}$ and $\langle\mathbf{v}^2\rangle \simeq \overline{\mathbf{v}^2}$.

Keeping the time evolution of $\overline{\boldsymbol{\mathcal{E}}}$ as a separate equation to couple into the theory and solve allows for oscillations and phase delays between extrema of field strength and extrema of $\overline{\boldsymbol{\mathcal{E}}}$ (Blackman and Field 2002) and are of observational relevance (as they have been used to explain the phase shift between spiral arms and dominant large scale mean field

magnetic polarization in the galaxy; Chamandy et al. 2013). But simulations of magnetic field evolution in the simplest forced isotropic helical turbulence reveal that a good match to the large scale magnetic field evolution can be achieved even when the left side of Eq. (23) is ignored and τ is taken as the eddy turnover time associated with the forcing scale. We adopt that approximation here and so Eq. (23) then gives

$$\overline{\mathcal{E}} = \alpha \overline{\mathbf{B}} - \beta \nabla \times \overline{\mathbf{B}}. \tag{25}$$

Equations (21) and (22) then become

$$\frac{1}{2}\partial_t \langle \overline{\mathbf{a} \cdot \mathbf{b}} \rangle = -\alpha \langle \overline{B}^2 \rangle + \beta \langle \overline{\mathbf{B}} \cdot \nabla \times \overline{\mathbf{B}} \rangle - \nu_M \langle \overline{\mathbf{b} \cdot \nabla \times \mathbf{b}} \rangle \tag{26}$$

and

$$\frac{1}{2}\partial_t \langle \overline{\mathbf{A}} \cdot \overline{\mathbf{B}} \rangle = \alpha \langle \overline{B}^2 \rangle - \beta \langle \overline{\mathbf{B}} \cdot \nabla \times \overline{\mathbf{B}} \rangle - \nu_M \langle \overline{\mathbf{B}} \cdot \nabla \times \overline{\mathbf{B}} \rangle. \tag{27}$$

The energy associated with the small scale magnetic field does not enter $\overline{\mathcal{E}}$ (Gruzinov and Diamond 1996) so it does not enter Eqs. (26) and (27). It arises as a higher order hyper diffusion correction (Subramanian 2003) which we ignore. However, the energy density in the large scale field $\propto \overline{B}^2$ *does* enter (26) and (27). In general we need a separate equation for the energy associated with the energy of the mean field. Fortunately, for the simplest α^2 dynamo discussed in Sect. 4.2 below, the non-helical large scale field does not grow even when the additional equation is added. And for the decay problem of Sect. 4.3, the non helical part of the magnetic energy decays very rapidly. As such, it is acceptable to assume that the large scale field is fully helical for present purposes.

The essential implications of the coupled Eqs. (26) and (27) for a closed or periodic system are revealed in standard approaches where the large scale overbarred mean magnetic quantities are now indicated with subscript "1", small scale quantities by subscript "2". The kinetic forcing scale is indicated by subscript f. In the usual two-scale model for the α^2 dynamo, the kinetic forcing wavenumber k_f is assumed to be same as that for the small scale magnetic fluctuations k_2. Relaxing this provides some versatility, but we take $k_f = k_2$ here for simplicity. We assume that the wave number k_1 associated with the spatial variation scale of large scale quantities satisfies $k_1 \ll k_2$, where k_2 is the wave number associated with small scale quantities. Applying these approximations to a closed or periodic system, we then use $\langle \overline{\mathbf{B}} \cdot \nabla \times \overline{\mathbf{B}} \rangle = k_1^2 \langle \overline{\mathbf{A}} \cdot \overline{\mathbf{B}} \rangle \equiv k_1^2 H_1$, $\langle \overline{\mathbf{B}}^2 \rangle = k_1 |H_1|$, along with $\langle \mathbf{b} \cdot \nabla \times \mathbf{b} \rangle = k_2^2 \langle \mathbf{a} \cdot \mathbf{b} \rangle = k_2^2 H_2$. We will assume that $H_1 \geq 0$ for the example cases studied below.

Non-dimensionalizing by scaling lengths in units of k_2^{-1}, and time in units of τ, where we assume $\tau = (k_2 v_2)^{-1}$, we have

$$h_1 \equiv \frac{k_2 H_1}{4\pi\rho v_2 2}, \qquad h_2 \equiv \frac{k_2 H_2}{4\pi\rho v_2^2}, \qquad h_v \equiv \frac{H_V}{k_2 v_2^2}, \qquad R_M \equiv \frac{v_2}{\nu_M k_2}.$$

With these non-dimensional quantities, Eqs. (26) and (27) become

$$\partial_\tau h_1 = \frac{2}{3}(h_2 - h_v)\frac{k_1}{k_2}h_1 - \frac{2}{3}\left(\frac{k_1}{k_2}\right)^2 h_1 - \frac{2}{R_M}\left(\frac{k_1}{k_2}\right)^2 h_1, \tag{28}$$

$$\partial_\tau h_2 = -\frac{2}{3}(h_2 - h_v)\frac{k_1}{k_2}h_1 + \frac{2}{3}\left(\frac{k_1}{k_2}\right)^2 h_1 - \frac{2}{R_M}h_2. \tag{29}$$

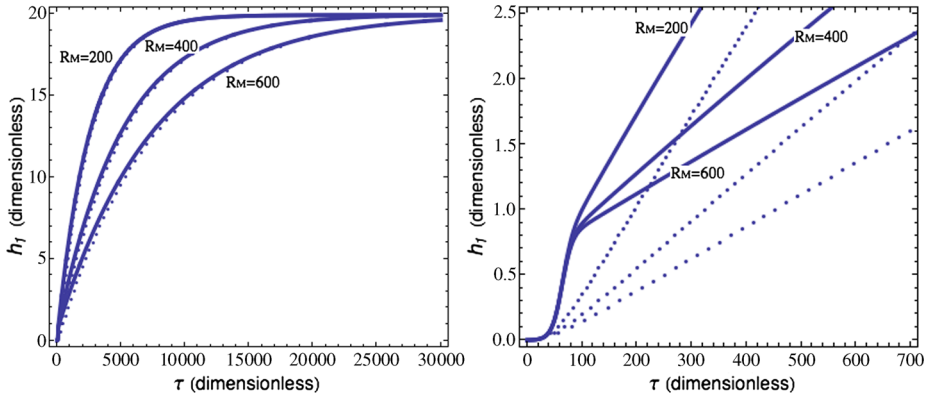

Fig. 9 Solutions of Eqs. (28) and (29) for the α^2 dynamo problem discussed in the text (figs. based on Field and Blackman 2002 and Blackman and Field 2002). The calculation maintains $h_v = -1$ and the initial conditions are $h_2(0) = 0$ and $h_1(0) = 0.001$ and for three different magnetic Reynolds numbers as shown (order of R_M in the *solid curves* are the same for the right curves as the left). Time (x-axis) is in units of eddy turnover times at the forcing scale $k = 5$. *Left panel* shows the solution over a long time period highlighting the analytical result that all curves eventually converge toward the same final value of h_1, but the higher R_M cases (those which are slower to dissipate the offending small scale magnetic helicity) take longer to get there. The *dotted curves* show the quasi-empirical fit formula used by Brandenburg (2001) to fit simulations at late times. The dynamical theory of Eqs. (28) and (29) do very well to match this empirical fit formula which in turn matched simulations. *Right panel* shows the solution only through $\tau = 700$. This highlights that at early times, before h_2 has grown significantly, the growth of h_1 is independent of R_M. The *dotted lines* are the *artificial* extension of the empirical fit formula of Brandenburg (2001) beyond its region of validity. The R_M dependence of the dynamical solution only arises at late times, and the empirical fit formula is only applicable in the R_M dependent regime

Equations (28) and (29) comprise a powerful set for capturing basic helicity dynamics for closed or periodic volume low lowest order in turbulent anisotropy. They help to conceptually unify a range of physical process depending on the initial conditions. Examples are described in the next subsections.

4.2 Large Scale Field Growth: The α^2 Dynamo Example

Consider a closed or periodic system with an initially weak seed large scale magnetic helicity at wave number k_1, with initially $0 < h_1(\tau = 0) \ll 1$, and with $h_2(\tau = 0) = 0$. Suppose the system is steadily forced isotropically with kinetic helicity at wave number $k_2 \gg k_1$ such that $h_v = -1$ in Eqs. (28) and (29). Solutions to this problem are shown for different time ranges as the solid lines in Fig. 9(left and right panels) for $k_2/k_1 = 5$ and three different magnetic Reynolds numbers (as in Field and Blackman 2002 rather than Blackman and Field 2002 since $\partial_t \overline{\boldsymbol{\mathcal{E}}}$ is ignored).

The basic interpretation of the curves is this: At early times, the R_M dependent terms in Eqs. (28) and (29) are small and h_1 grows exponentially with a growth rate $\gamma = \frac{2k_1}{3k_2}(h_v - \frac{k_1}{k_2})$ from Eq. (28). The first three terms on the right of Eq. (29) have the same magnitude but opposite sign as those on the right of Eq. (28), so h_2 grows with opposite sign as h_1 with the same growth rate during this kinematic, R_M independent growth phase. This phase lasts until the compensating growth of h_2 becomes large enough to significantly offset the driving from h_v and reduce γ to a level for which the R_M terms become influential. The R_M term of Eq. (28) is k_2^2/k_1^2 times that Eq. (29), so h_2 is quenched by its R_M term earlier, allowing h_1 to continue growing, albeit now at an R_M dependent rate. In the $R_M \gg 1$ limit, the growth rate

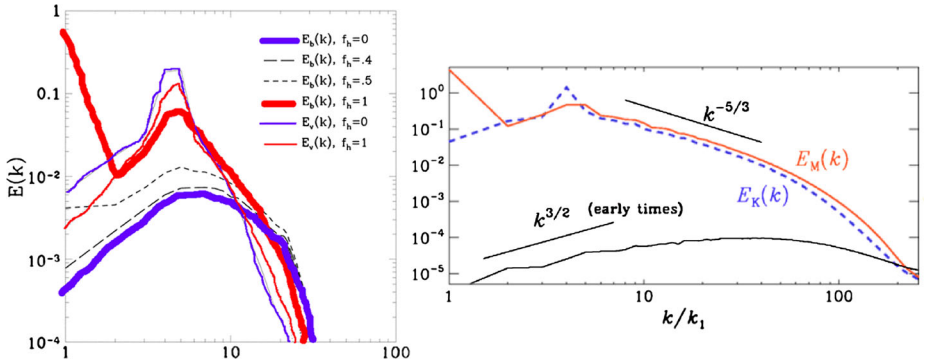

Fig. 10 Example steady-state saturated spectra from direct numerical simulations of helically forced MHD turbulence. The *left panel* is adapted from Maron and Blackman (2002) for 64^3 simulation and magnetic Prandtl number 3 with forcing wavenumber $k = 5$. The *thick red* and *blue lines* are the magnetic and kinetic energy spectra for fractional kinetic helicity $f_h = 1$. The *thin red* and *blue lines* are the magnetic and kinetic energy spectra for $f_h = 0$. Large scale field growth (at $k = 1$) is dramatic in the $f_h = 1$ case and negligible for $f_h = 0$. The *right panel* is a 512^3 simulation for $f_h = 1$ for unit magnetic Prandtl number and forcing wavenumber $k = 4$ from Brandenburg et al. (2012). In the *right panel*, *blue* indicates kinetic energy and *red* indicates magnetic energy. The *thick* and *thin red lines* of the *left panel* thus correspond respectively to the *red* and *blue lines* of the *right panel* in that these are all for the case of $f_h = 1$. The *right panel* also shows large scale $k = 1$ field for helical forcing. The essential features of the growth of the large scale field to saturation in such simulations are captured by Eqs. (28) and (29) the solutions of which are shown in Fig. 9

past the initial R_M independent regime is extremely small and generally not astrophysically relevant.

At the end of the kinematic phase, it can be shown analytically that the energy in the helical field grows to $B_1^2 \sim k_1 H_1 = \frac{k_1}{k_2}(1 - \frac{k_1}{k_2})v_2^2$. At this point the three different R_M curves in Fig. 9(right panel) diverge with the lowest R_M curve being the faster to reach the asymptotic steady state. By setting the left sides of Eqs. (28) and (29) to zero, the asymptotic saturation value can be shown to be $B_1^2 = k_1 H_1 = \frac{k_2}{k_1}(1 - \frac{k_1}{k_2})v_2^2$, or $h_1 = 20$ for $k_2 = 5k_1$ as seen in Fig. 9(left panel). The final value of h_1 is independent of R_M even though the time to get there is longer for larger R_M.

In Fig. 9(left panel), the dotted lines represent an R_M dependent empirical fit formula to the late time data in numerical simulations of Brandenburg (2001) of the α^2 dynamo. The agreement between the solutions to Eqs. (28) and (29) and the empirical fit formula to the simulations is quite good at late times. The dotted lines Fig. 9(right panel) represent the *artificial extension* of this empirical fit formula to early times where it does not apply. The asymptotic regime has an R_M dependence whereas the early time regime does not. More recent simulations (Brandenburg 2009) have confirmed that the large scale growth rate varies by only 16 % in the kinematic regime when R_M varies by a factor of 100. The success of these two simple equations in capturing saturation features of dynamo simulations highlights the importance of coupling magnetic helicity into the dynamics of field growth.

Examples of the large scale magnetic and kinetic energy spectra for the α^2 dynamo from direct numerical simulations in a periodic box starting with an initial weak seed field and forced with helical forcing at $k = 5$ are shown in Fig. 10. The left panel shows a 64^3 simulation and the saturated end state of magnetic and kinetic energies for different forcing fractions of kinetic helicity $f_h = |\langle \mathbf{v} \cdot \nabla \times \mathbf{v} \rangle| / k_f \langle \mathbf{v}^2 \rangle$ and magnetic Prandtl number $= 3$ from Maron and Blackman (2002). In the left panel, the thick red and blue lines are the magnetic and kinetic energy spectra for the case of $f_h = 1$. The thin red and blue lines are the mag-

netic and kinetic energy spectra for the case of $f_h = 0$. The right panel is a 512^3 simulation from Brandenburg et al. (2012) for $f_h = 1$ for unit magnetic Prandtl number. In the right panel, blue indicates kinetic energy spectrum and red indicates magnetic energy spectrum. The thick and thin red lines of the left panel thus correspond respectively to the red and blue lines of the right panel in that these are all for the case of $f_h = 1$. Both panels show the dramatic emergence of the large scale $k = 1$ field for helical forcing. The thick blue curve in the left panel shows the absence of the large scale $k = 1$ magnetic field for $f_h = 0$.

4.3 Helical Field Decay

A second use of Eqs. (28) and (29) is to study how helical fields decay. As alluded to earlier, when a magnetic activity cycle period with field reversals is evident, the need for an in situ LSD is unambiguous. But when no cycle period is detected, the question of whether otherwise inferred large scale fields are LSD produced or merely a fossil field often arises. The question of how efficiently magnetic fields decay in the presence of turbulence is important because if a fossil field would have to survive this diffusion to avoid the need for an in situ dynamo.

Most work on the diffusion of large scale fields has not distinguished between the diffusion of helical vs. non-helical large scale fields. Yousef et al. (2003) and Kemel et al. (2011) found that fully helical large scale fields decay more slowly than non-helical large scale fields in numerical simulations. Blackman and Subramanian (2013, hereafter BS13) analyzed (28) and (29) for the field decay problem and identified a critical helical large scale magnetic energy above which decay is slow and below which decay is fast when the small scale helicity h_2 is initially zero. Bhat et al. (2014) further developed this theory and tested the results with numerical simulations and emphasized a distinction between two problems: the case studied by BS13 and the case in which the initial field decays slowly and then it transitions to fast decay.

The basic result in BS13 is captured by the solution to Eqs. (28) and (29) for initial conditions for which $h_1 > 0$, $h_2 = 0$, $h_v = 0$. This corresponds to a case in which there is no kinetic helicity, just a driving turbulent kinetic energy that causes turbulent diffusion of h_1 through the penultimate term on the right of Eq. (28). The question studied is how does h_1 evolve for these circumstances as a function of its initial value? The solutions are shown in Fig. 11 adapted form Bhat et al. (2014). From top to bottom the curves correspond to the initial values of large scale helical field energy $k_1 h_{1,0}/k_2$ in units of equipartition with the turbulent kinetic energy. For the chosen ratio $k_2/k_1 = 5$, the value $k_1 h_{1,0}/k_2 = 0.04 = (k_1/k_2)^2$ and marks a threshold initial value below which $k_1 h_1/k_2$ decays rapidly via turbulent diffusion and above which it decays restively slowly (actually, at twice the resistive diffusion rate). Since $k_1 h_1/k_2$ is the dimensionless magnetic energy associated with h_1, the energy in the helical field need only be at least k_1^2/k_2^2 times that of the turbulent kinetic energy to avoid fast decay. The implication is that helical field energy above a modest value decays resistively slowly even in the presence of turbulent diffusion. This contrasts the behavior of the non-helical part of the large scale magnetic, which always decays at the turbulent diffusion rate independent of the presence or absence of a helical component (BS13).

Why should the helical field resist turbulent diffusion and what determines the critical value? The answer is as follows (BS13; Bhat et al. 2014): Slow decay of h_1 occurs when the last term on the right of (28) is no smaller than the sum of the first two terms on the right ($h_v = 0$ for the present case). For large R_M, each of those first two terms is separately much larger than the last term so their combination would have to nearly cancel to meet the aforementioned condition. These same terms also appear in the equation for h_2 with

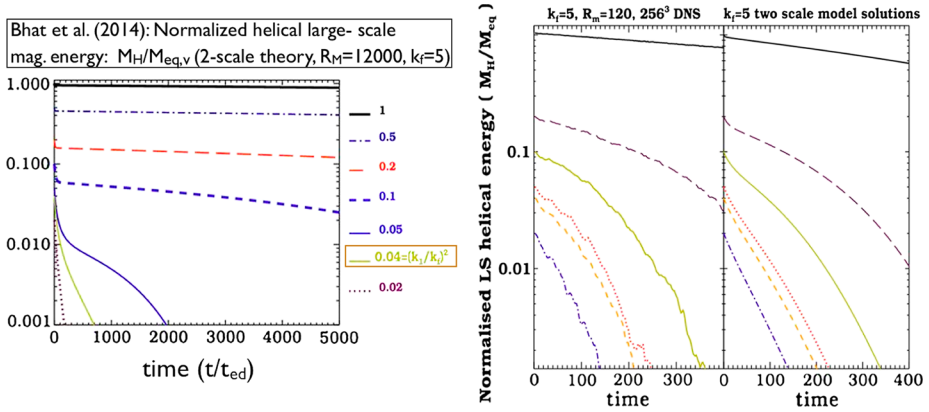

Fig. 11 Figure is from Bhat et al. (2014) and addresses the resilience of large scale helical fields to decay. The *left panel* shows solutions of Eqs. (28) and (29) for $M = k_1 h_1/k_2$, non-dimentionalized to the turbulent equipartition value and for the initial values shown, subjected to steady turbulent forcing with $h_v = 0$. Slow decay occurs when initially $h_1 > k_1/k_2$ and fast decay occurs when the initial value is below this value. The critical value of M is boxed in yellow. In the *left panel*, $k_2/k_1 = 5$ and $R_M = 12000$. The *right panel* shows a comparison between simulations and theory for the same problem at lower R_M. The agreement looks good. A subtlety however, is that the R_M accessible in the simulations is too low to identify the transition value $h_1 = k_1/k_2$ (see text of Sect. 4.3)

opposite sign. Initially, $h_1 > 0$ and $h_2 = 0$ and if we seek the initial value of h_1 for slow decay, we note that slow decay can only occur after a very rapid evolutionary phase (with negligible dependence on R_M) where a swift buildup of h_2 leads to an approximate balance between these aforementioned two terms. The needed amount of h_2 to abate decay of h_1 can be estimated by balancing first two terms on the right of either (28) or (29) for our case of $h_v = 0$. This gives $h_2 \sim (k_1/k_2)$. But since the only source of h_2 is h_1, this value of h_2 is also the minimum value of the initial $h_{1,0}$ needed for slow decay of h_1. That is, $h_{1,0} > h_c \equiv k_1/k_2$ for slow decay.

A qualitative comparison between the numerical simulations and the analytic solutions for the case just described is shown in Fig. 9(right panel). The behavior in the simulations looks similar to that of the analytic model. The one caveat is that the simulations do not achieve the resolution needed to ensure that the last term of Eq. (27) is smaller than the penultimate term for h_1 near the small critical value of k_1/k_2. However, as mentioned above, in addition to the case just described where the threshold initial value of h_1 for slow decay is sought, Bhat et al. (2014) also studied the case for which the field is initially above the threshold for slow decay and later transitions to fast decay. In that case they show that the value of h_1 at the transition is independent of k_1/k_2, unlike the case discussed above. In this second case, h_2 has already saturated by the time h_1 makes the transition to fast decay and so the estimate of the threshold of h_2 (and thus h_1) for the previous case does not apply. This result and the distinction between the two cases are both contained within the analytic framework of Eqs. (28) and (29) as discussed in Bhat et al. (2014) where theory and simulation are shown to agree. Confidence in the overall theory and physical interpretation of both cases is bolstered by this correspondence.

Taken at face value, the survival of helical fields to turbulent diffusion may provide rejuvenated credence to pre-galactic mechanisms of large scale field production that produce sufficiently strong helical fields (Field and Carroll 2000; Copi et al. 2008; Díaz-Gil et al. 2008; Semikoz et al. 2012; Tevzadze et al. 2012; Kahniashvili et al. 2013)

because such helical fields could then avoid decay by supernova driven turbulent diffusion over a galactic lifetime in the absence of boundary terms. Although most energy in large scale galactic magnetic fields resides in non-helical toroidal fields, as long as the turbulent decay time for the non-helical field exceeds the linear shear time, we can expect a predominance of non-helical field in a steady state, even without an in situ dynamo to regenerate the poloidal fields: The helical field provides a minimum value below which the toroidal field cannot drop. The toroidal field enhancement over the poloidal field would be that which can be linearly shear amplified in a non-helical field diffusion time. Similar considerations regarding the survival of helical fields could apply for the large scale fields of stars and accretion disks.

Another implication of slow diffusion of helical fields is that the observation of a helical large scale field in jets from Faraday rotation (Asada et al. 2008; Gabuzda et al. 2008, 2012) does not guarantee magnetic energy domination (Lyutikov et al. 2005) on the observed scales (BS13).

The calculations just discussed do not include buoyancy or other boundary loss terms that could extract large scale helicity at a rate that may still need to be re-supplied from within the rotator. If such terms are important, then both helical and non-helical large scale fields would deplete, and an in situ dynamo would be needed for replenishment. But this shifts the focus from turbulent diffusion to that of boundary loss terms in assessing the necessity of in situ dynamos. More on flux and boundary terms will be discussed in the next section.

4.4 Dynamical Magnetic Relaxation

The resilience of helical fields to turbulent diffusion of the previous section is actually the result of the current helicity part of the α effect in the language of dynamo theory rather than an intrinsic change of the diffusion coefficient β. In this respect, the resilience of large scale helical field to decay is very rooted in the basic principles of Sect. 2. Namely, magnetic helicity has the lowest energy when on the largest scale. Diffusing it to small scales while conserving magnetic helicity is fighting against this relaxation.

In fact we can also use Eqs. (28) and (29) to study yet a different problem. Starting with $h_1 \ll 1$ and $h_2 \gg h_1$, and $h_v = 0$ we can solve for the evolution of h_1. Indeed, Blackman and Field (2004). Kemel et al. (2011), and Park and Blackman (2012) carried out such calculations using versions of Eqs. (28) and (29) where the system is initially driven with h_2 and found that it does indeed capture the dynamical relaxation of magnetic helicity to large scales: h_1 grows exponentially as the helicity is transferred from h_2. In this case, the large scale field grows with the same sign as h_2, and the combination of the turbulent diffusion and a modestly growing h_v emerge as the back reactors, contrasting the α^2 dynamo case of Sect. 4.2 above.

Although the dynamics of magnetic helicity and dynamical relaxation have often not been explicitly discussed in the context of fossil field origin models of stars (Braithwaite and Spruit 2004), the same basic principles are prevalent.

5 Helicity Fluxes

The previous section did not include the role of flux or boundary terms in the evolution equations. While the role of helicity fluxes in sustaining magnetic relaxation dynamos in laboratory fusion plasmas has been long-studied as essential (Strauss 1985, 1986; Bhattacharjee and Hameiri 1986; Bellan 2000) the awareness of its importance for astrophysical contexts

has emerged more recently (Blackman and Field 2000a, 2000b; Vishniac and Cho 2001; Blackman 2003; Shukurov et al. 2006; Käpylä et al. 2008; Ebrahimi and Bhattacharjee 2014).

Laboratory plasma helical dynamos in a reversed field pinch (RFP, Ji and Prager 2002) for example, typically involve a magnetically dominated initial state with a dominant mean magnetic toroidal magnetic field. When an external toroidal electric field is applied along this torioidal field, a current is driven along the magnetic field which injects magnetic helicity of one sign on small scales. This generates a poloidal field. For sufficiently strong applied electric fields, the system is driven far enough from its relaxed state that helical tearing or kink mode instabilities occur. The consequent fluctuations produce a turbulent EMF $\overline{\boldsymbol{\mathcal{E}}}$ that drives the system back toward the relaxed state. As discussed in Sect. 2, the relaxed state is the state in which the magnetic helicity is at the largest scale possible, subject to boundary conditions. When the helicity injection is externally sustained, a dynamical equilibrium with oscillations can incur as the system evolves toward and away from the relaxed state. The time-averaged $\overline{\boldsymbol{\mathcal{E}}}$ is maintained by a spatial (radial) flux of small scale magnetic helicity within the plasma. The injection of helicity is balanced by the dynamo relaxation, so the dynamo sustains the large scale field configuration against decay.

The simplest circumstance revealing the importance of flux terms is a steady state for which the left hand side of Eqs. (21) and (22) vanish. Then, if divergences do not vanish, the magnetic field aligned EMF would be sustained by helicity fluxes, whose divergences are equal and opposite for the large and small scale contributions, that is

$$0 = 2\langle \overline{\boldsymbol{\mathcal{E}}} \cdot \overline{\mathbf{B}} \rangle - c\nabla \cdot \langle \overline{\phi}\overline{\mathbf{B}} + \overline{\mathbf{E}} \times \overline{\mathbf{A}} \rangle \tag{30}$$

and

$$0 = -2\langle \overline{\boldsymbol{\mathcal{E}}} \cdot \overline{\mathbf{B}} \rangle - c\nabla \cdot \langle \phi\mathbf{b} + \mathbf{e} \times \mathbf{a} \rangle. \tag{31}$$

Combining these two equations reveals that the divergences of large and small scale helicity through the system are equal in magnitude but oppositely signed.

The specific observational interpretation of flux divergence terms depends on the averaging procedure. If the averaging is taken over the entire interior of a rotator such as a star or disk, then such non-zero fluxes in a steady-state would imply equal magnitude but oppositely signed rates of large and small scale magnetic helicity flow through the boundary into the corona (Blackman and Field 2000b). In a steady state, each hemisphere would receive both signs of magnetic helicity but the respective signs on large and small scales would be reversed in the two hemispheres.

Complementarily, Blackman (2003, Fig. 9 therein) showed how an imposed preferential small scale helicity flux could reduce quenching in the α^2 dynamo and the result is shown in Fig. 12 to a larger value of R_M. A simple term of the form $-\lambda h_2$ was added to Eq. (29) to make these plots and solutions for different values of λ are shown. The left panel shows the late time saturation value is increased with increasing λ and the right panel shows the tendency that for large enough λ the kinematic regime (the regime independent of R_M) can be extended. Del Sordo et al. (2013) have studied numerically the relative role of advective and diffusive fluxes. Their generalized α^2 dynamos can become oscillatory with even a weak advective wind, due to the spatial dependence of the imposed kinetic helicity. They do indeed find that for $R_M > 1000$ the advective flux dominates the diffusive flux and helps alleviate the resistive quenching. However predicting analytically the exact value of the critical R_M where this occurs requires further work.

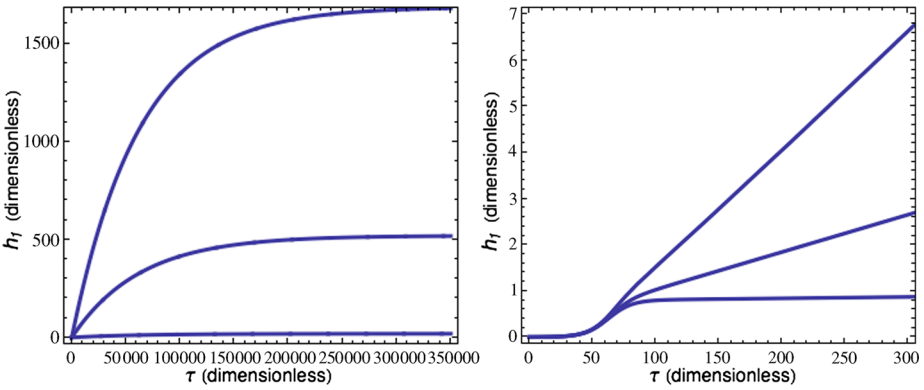

Fig. 12 Figure updated from Blackman (2003): This shows the conceptual role of a simple advective type helicity flux in increasing the h_1 saturation value of the α^2 dynamo, and the trend toward extending the growth of h_1 before resistive quenching incurs. The *three curves* in each panel correspond solutions of Eqs. (28) and (29) modified by the addition of a loss term $-\lambda h_2$ to Eq. (29). All curves correspond to $R_M = 5000$. From top to bottom in each panel the curves have $\lambda = 1/30, 1/100$ and 0 respectively. *Left panel* is the late time regime: The *bottom curve* saturates at the same value as those in Fig. 9(left panel), as those have no loss term (although Fig. 9(left panel) has faster growth because the R_M values are smaller). The *right panel* is the early time regime, and shows that for $\lambda = 1/30$ the resistive turnover in the h_1 curve is nearly avoided. This holds true even more dramatically for all larger values of λ (not shown)

5.1 Helicity Fluxes in Galactic and Stellar Contexts

The α^2 dynamo has no shear but helicity flux in the presence of shear is particularly important because generalizations of Eqs. (28) and (29) to the $\alpha - \Omega$ LSD otherwise lead to large scale field decay. Figure 12 can be contrasted with Fig. 13 in this regard. Figure 13 shows the results of Shukurov et al. (2006) for a model of the Galactic dynamo. The equations shown represent the generalization of Eqs. (28) and (29) to the $\alpha - \Omega$ dynamo with only vertical z derivatives retained and with an advective flux term that ejects small scale magnetic helicity from the system. The figure shows that the large scale field decays when this flux is too small, illustrating its important role in sustaining the EMF. In the solar context, a similar circumstance arises: Käpylä et al. (2008) found from simulations that an LSD is produced by convection + shear when surfaces of constant shear were aligned toward open boundaries allowing a helicity flux whereas Tobias et al. (2008) found no LSD when shear was aligned toward periodic boundaries disallowing helicity fluxes.

The role and potential observability of such global helicity fluxes are exemplified schematically in Fig. 14, originally in the context of the sun (Blackman and Brandenburg 2003). The figure illustrates the same principles as the comparison between Figs. 7 and 8 but with shear and buoyancy. In the northern hemisphere, the field exhibits a right handed writhe and a left handed small scale twist as the structure buoyantly emerges into the corona. The emergent separation of scales of magnetic helicity was verified by simulation of a buoyant, writhed tube. Such structure might in fact be evident in the TRACE image of coronal loop shown in Fig. 15 (from Gibson et al. 2002). The figure shows left hand twist and right handed writhe. A key point is that such ejections could be an essential part of sustaining the fast solar cycle, not just an independent consequences of magnetic field generation.

This segregation of helicity signs is consistent with other evidence that the northern hemisphere exhibits primarily small scale left handed twist and larger scale right handed writhe, with these reversed in southern hemisphere (Rust and Kumar 1996; Pevtsov et al. 2008;

Shukurov et al. (2006):

$$\mathcal{E} = \alpha \overline{B} - \eta_t \overline{J}$$

$$\alpha = \alpha_K + \alpha_m$$

$$\alpha_m = \tfrac{1}{3}\rho^{-1}\tau \overline{j \cdot b}$$

Unlike the α^2 dynamo, the α-Ω dynamo may catastrophically quench without fluxes if driven initially by α_K

$$\frac{\partial \overline{B}_r}{\partial t} = -\frac{\partial}{\partial z}\left(\overline{U}_z \overline{B}_r + \mathcal{E}_\phi\right) + \eta \frac{\partial^2 \overline{B}_r}{\partial z^2},$$

$$\frac{\partial \overline{B}_\phi}{\partial t} = -\frac{\partial}{\partial z}\left(\overline{U}_z \overline{B}_\phi - \mathcal{E}_r\right) + \eta \frac{\partial^2 \overline{B}_\phi}{\partial z^2} + q\Omega_0 \overline{B}_r,$$

$$\frac{\partial \alpha_m}{\partial t} = -2\eta_t k_0^2 \left(\frac{\mathcal{E} \cdot B}{B_{eq}^2} + \frac{\alpha_m}{R_m}\right) - \nabla \cdot \left(\alpha_m \overline{U}\right)$$

$$\overline{B}_r = \overline{B}_\phi = 0 \quad \text{at } z = \pm h.$$

$$C_U = \frac{U_0}{\eta_t k_1}, \quad C_\Omega = \frac{\Omega_0}{\eta_t k_1^2}, \quad C_\alpha = \frac{\alpha_0}{\eta_t k_1}$$

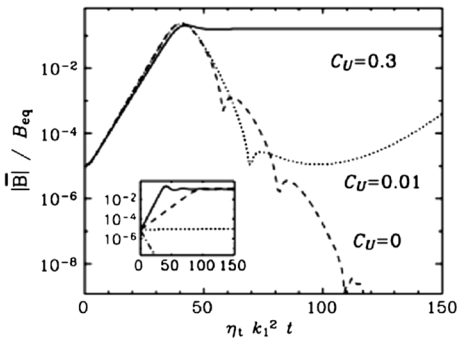

Fig. 13 From Shukurov et al. (2006), this provides a simple model illustrating the importance of helicity fluxes in sustaining the $\alpha - \Omega$ dynamo when magnetic helicity dynamics and fluxes are coupled into the theory. They considered an advective contribution to the helicity flux, as shown boxed in *red*, and quantified its contribution by C_U. The *plots on the right* show that only above a threshold value of C_U does the large scale mean field (plotted in units of the field strength corresponding to equipartition with the turbulent kinetic energy) sustain. Without these fluxes, the field decays. This contrasts the situation of the α^2 dynamo in Fig. 12 in which flux terms increase the saturation value but do not determine the difference between growth and decay

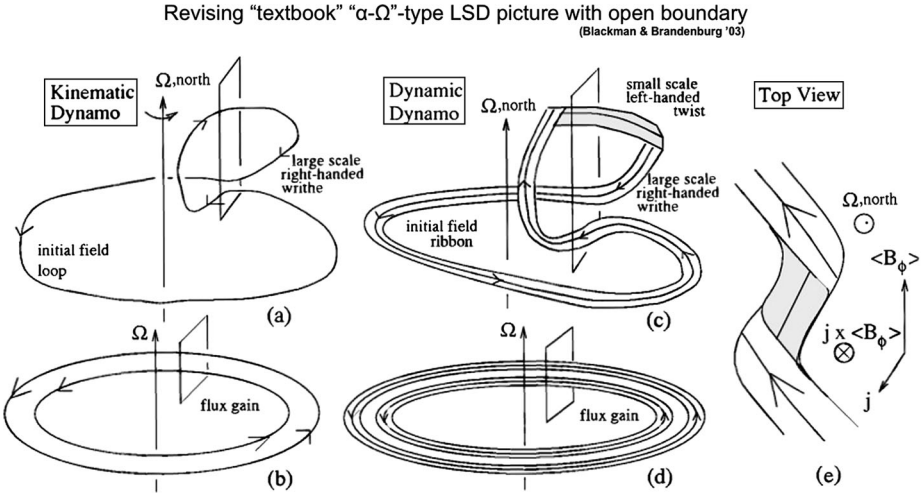

Fig. 14 From Blackman and Brandenburg (2003), a comparison of the classic picture of $\alpha - \Omega$ dynamo without magnetic helicity conservation (panel (**a**)) to that with magnetic helicity conservation (panel (**c**)). Panels (**b**) and (**d**) show the gain in toroidal field after ejection of the large poloidal loop. For panel (**d**), this ejection alleviates the twist that would otherwise build up. This figure is a conceptual generalization of the concepts addressed by the comparison of Figs. 7 and 8 to include shear and buoyancy and to motivate why e.g. coronal mass ejections of the sun, or galaxies may represent the irreversible loss of small scale magnetic helicity that allows LSD action to sustain. See also Fig. 13

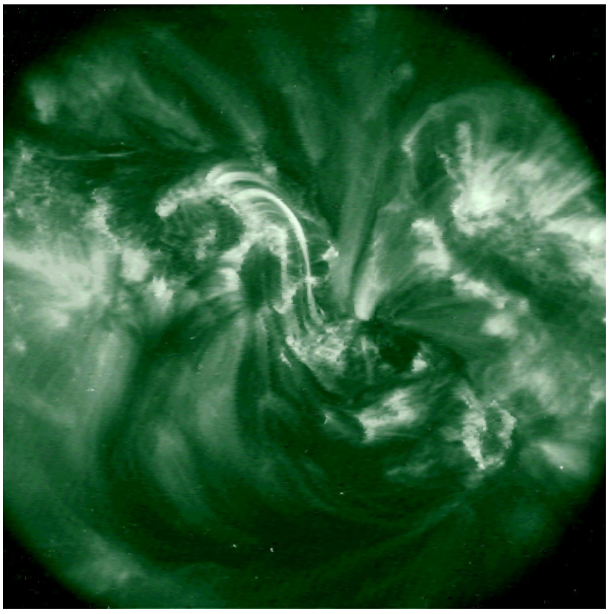

Fig. 15 TRACE 195 Å image of a solar sigmoid of the Northern hemisphere from Gibson et al. (2002). It is tempting to interpret the large scale right-handed writhe and small scale left handed striations along the sigmoid being consistent with what a magnetic helicity conserving dynamo would predict when the fluxes eject both small and large scale helicities from the interior. The ejection of the small scale helicity in sigmoids or coronal mass ejections may be fundamental to the operation of the solar dynamo, not just a consequence of large scale field generation

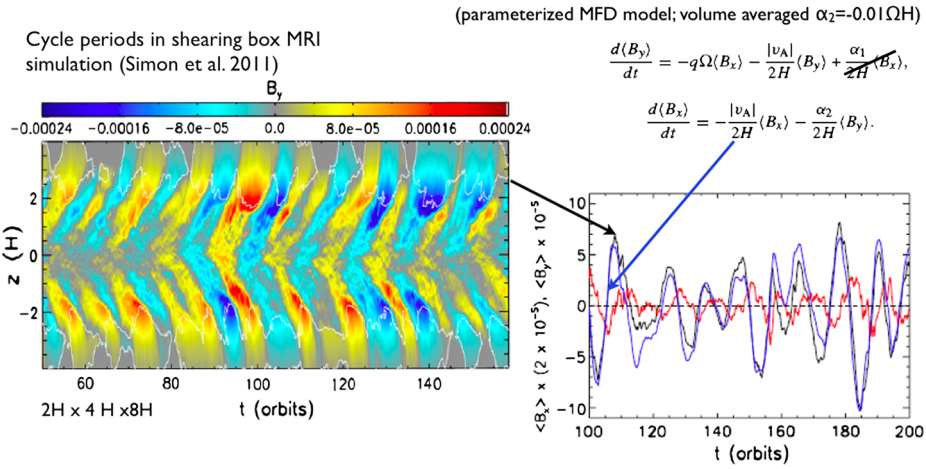

Fig. 16 Example of evidence for large scale dynamo action in MRI simulations from Simon et al. (2011), compared with an empirically tuned $\alpha - \Omega$ dynamo model. The *left panel* shows the net torioidal field vs. time, volume averaged over all x and y and over $|z| < 0.5H$. Outflow vertical boundaries were used and periodic boundaries in the other two dimensions. The cycle period of ~ 10 orbits is evident. The *black line* in the *right panel* shows the mean toroidal field as function of time and the *blue line* corresponds to the model semi-empirical fit equation of the $\alpha - \Omega$ dynamo. The sign of the required dynamo α coefficient is opposite to that expected from kinetic helicity

Zhang et al. 2010; Hao and Zhang 2011). These features seem to be invariant with respect to solar cycle, as would be predicted by helical dynamos, even when the field itself reverses sign. Note also that $H\alpha$ filaments seem to exhibit "dextral" (right handed) twist in North

and "sinstral" (left handed) in south (Martin and McAllister 1997) BUT: right handed $H\alpha$ filaments may be supported by left handed fields and vice versa (Rust 1999).

There have been efforts to measure the rate of injection of magnetic helicity (Chae et al. 2004; Schuck 2005; Lim et al. 2007), particularly, its gauge invariant cousin: the "relative magnetic helicity" (Berger and Field 1984; the difference between actual magnetic helicity and that of a potential field) by tracking footprint motions. It can be shown that the footpoint motions provide a direct measure of this input rate (Démoulin and Berger 2003). There have also been efforts to relate the current helicity to the injection rate of magnetic helicity (Zhang et al. 2012). Ultimately, measuring the detailed spectra of current helicity and relative magnetic helicity injection into the corona and solar wind (Brandenburg et al. 2011) is a highly desirable enterprise for the future. Commonly, observational work has focused on the component of twist with the current along the line of sight, but measuring the full current and magnetic helicities require all three components of the field.

5.2 Helicity Fluxes in Accretion Disks and Shearing Boxes

Essentially all MRI unstable simulations with large enough vertical domains, whether stratified, unstratified, local or global, show the generation of large scale toroidal fields of the same flux for cycle periods of ~ 10 orbits (Brandenburg et al. 1995; Lesur and Ogilvie 2008; Davis et al. 2010; Simon et al. 2011; Guan and Gammie 2011; Sorathia et al. 2012; Suzuki and Inutsuka 2013; Ebrahimi and Bhattacharjee 2014). The patterns indicate a large scale dynamo operating contemporaneously with the small scale dynamo. The key unifying property of all of these cases is mean field aligned EMF, that is $\langle \overline{\boldsymbol{\mathcal{E}}} \cdot \overline{\mathbf{B}} \rangle$. The explicit form of $\overline{\boldsymbol{\mathcal{E}}}$ and the terms that contribute to it can depend on the boundary and stratification conditions and on the particular procedure for large scale averaging, but there is considerable similarity among the dynamos operating in these simulations. Sorting out whether and which flux terms are important for specific averaging and initial conditions is an ongoing task. To see the issues at hand, I highlight approaches to LSD modeling in shearing boxes without using helicity fluxes and then compare to those that do.

The left panel of Fig. 16, adapted from Simon et al. (2011) shows the toroidal magnetic field from a shearing box MRI simulation. The simulation used vertical stratification and periodic boundaries in the x and y (radial and azimuthal) and outflow boundaries in z (vertical) directions. The toroidal field was calculated by averaging over x and y and over $z \leq 5H$ where H is a density scale height. There was an initial net toroidal field in the box, but the left panel shows that the toroidal field reverses every 10 orbits in the saturated state. The right panel shows the use of model equations from an $\alpha - \Omega$ dynamo that Simon et al. (2011) adopted from Guan and Gammie (2011) tuned to match the simulation. The equations have only a shear term and a loss term from buoyancy in the torioidal field equation. The radial field equation has a buoyancy loss term and the $\alpha = \alpha_2$ dynamo term. There are no helicity dynamics in this empirical set of equations; those dynamics would at most y be hidden in the empirically determined α_2. Nevertheless, this quasi-empirical set of equations does well to model the field seen in the simulations.

In this example of Simon et al. (2011), like those of the first analyses of cycle periods in shearing box simulations (Brandenburg et al. 1995; Brandenburg and Donner 1997), the sign of the $\alpha = \alpha_2$ coefficient is found to be inconsistent with the standard 20th century textbook kinetic helicity. Additional features such as density stratification and rotation lead to higher order turbulent anisotropy and inhomogeneity that change the dominant sign of α appropriately (Rüdiger and Kichatinov 1993), and is consistent with the role of magnetic buoyancy (Brandenburg 1998). In this context, Gressel (2010) further looked at the behavior

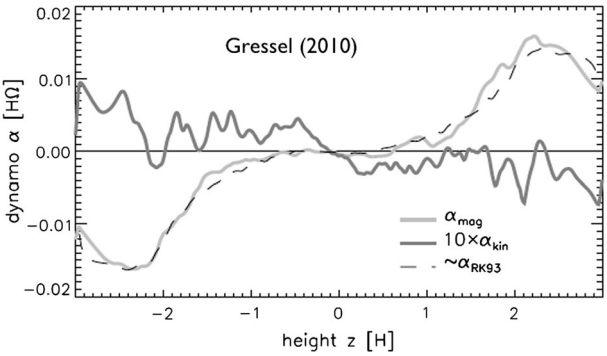

Fig. 17 Example of $\alpha - \Omega$ dynamo model for large scale fields compared to vertically stratified shearing box, MRI simulations from Gressel (2010). The vertical dependences of the α dynamo coefficients are shown. This coefficient is the proportionality between the EMF and the mean field (averaged in radius and azimuth). The values α_{kin} and α_{mag} are proportional to the kinetic and magnetic helcities respectively. The value α_{RK93} comes from Rüdiger and Kichatinov (1993) and is derived for stratified rotating turbulence. The figure shows that α_{RK93} or α_{mag} are much better fits to the dynamo in the shearing box than the traditional α_{kin} of 20th century textbooks. It would seem that α_{RK93} is therefore capturing the α_{mag} contribution and may result from magnetic buoyancy

of the dynamo α coefficient in stratified MRI shearing box (with outflow vertical boundaries) simulations and found that the sign of the dynamo α coefficient was consistent with the generalizations of Rüdiger and Kichatinov (1993), and also consistent with the sign of the current helicity correction term to α in Eq. (24), as if the current helicity contribution may be sourced by magnetic buoyancy. Gressel's results are shown in Fig. 17 and his averaging was taken over radius and azimuth.

The aforementioned approaches to MRI LSDs do not involve helicity fluxes, but calculations of EMF sustaining fluxes in this context have been emerging (e.g. Vishniac and Cho 2001; Vishniac 2009; Käpylä and Korpi 2011; Ebrahimi and Bhattacharjee 2014) (see also Vishniac and Shapovalov 2014 for an isotropically forced case with shear). In particular, Ebrahimi and Bhattacharjee (2014) studied an MRI unstable cylinder with conducting boundaries. They wrote down mean quantities averaged over azimuthal and vertical directions, leaving the radial direction unaveraged. They looked explicitly at the terms in the helicity conservation equation (21) and found that the electromotive force is well matched by the local flux terms measured from direct numerical simulations. Their results are shown in Fig. 18.

To calculate the specific form of these fluxes by brute force in a mean field theory involves expanding the fluctuating quantities in terms of mean field quantities via the dynamical equations for those fluctuating quantities and a closure (e.g. Brandenburg and Subramanian 2005). Such efforts are ongoing. One such flux that emerges from such a procedure that of Vishniac and Cho (2001). Ebrahimi and Bhattacharjee (2014) also plot this latter flux as seen in the let panel of Fig. 18. They find that it is much smaller than the total flux term directly calculated from the simulations, and thus is subdominant. Recall that Shukurov et al. (2006) in Fig. 13 considered an advective flux term that is another candidate flux term that emerges from mean field theory. Sur et al. (2007) also assessed the role of the Vishniac-Cho flux semi-analyticially in the galactic context and found it can be helpful if the mean magnetic field is above a threshold value to begin with. Vishniac and Shapovalov (2014) considered an isotropically forced periodic box with linear shear, (without the coriolis force) and find that the Vishniac-Cho flux is dominant. Their averaging procedure involves averaging over

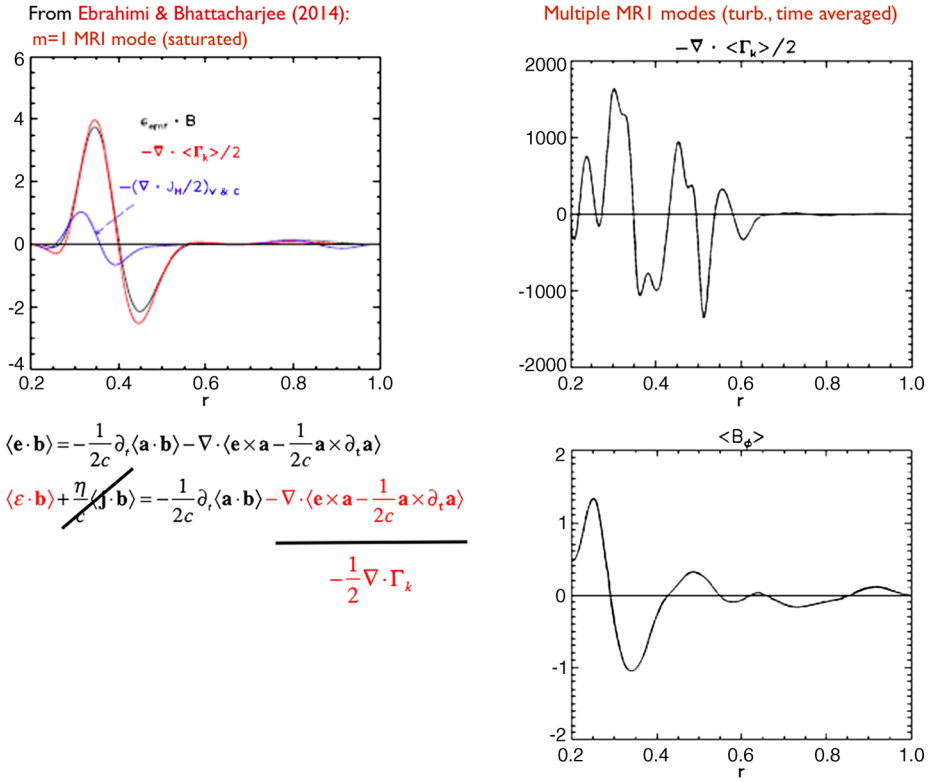

Fig. 18 Figures adapted from Ebrahimi and Bhattacharjee (2014), representing $R_M \gg 1$, and unit magnetic Prandtl number, shear flow driven simulations of an MRI unstable cylinder with perfectly conducting boundaries. This shows evidence for the generation of large scale field when averages are taken over height and azimuth, leaving the radial variable unaveraged. No initial net torioidal field was present in the box but one emerges as a result of LSD action. *Left panel*: Strong evidence for the importance of the radial flux of small scale magnetic helicity in sustaining the EMF needed for dynamo action for a single saturated unstable MRI mode is shown. The *black curve* is a measure of the field aligned EMF and the *red curve* is the helicity flux in shown in the equation. The *blue curve* is the Vishniac and Cho (2001) flux which is too small to match the total EMF sustaining flux. *Right pair of figures* shows the radial correspondence between the net toroidal field and helicity flux divergence additionally time-averaged for a turbulent state in which multiple MRI unstable modes interact. The correspondence provides further evidence for the importance of local helicity fluxes in sustaining the LSD

the entire box and filtering by wavenumber to distinguish contributions from mean and fluctuating components. This procedure is different from that of Ebrahimi and Bhattacharjee (2014) discussed above. See also Hubbard and Brandenburg (2011) however, who suggest that the choice of gauge influences whether the Vishniac-Cho flux is important in numerical simulations.

In general, the different circumstances and averaging procedures of mean field quantities between simulations of e.g. Simon et al. (2011), Ebrahimi and Bhattacharjee (2014) and those of Vishniac and Shapovalov (2014) highlight the need for clarity in tailoring the specific mean field theory to capture the dominant contributions for different combinations of forcing, boundary conditions, and averaging procedures. There is also an opportunity to combine mean field theories for local transport (e.g. Ogilvie 200; Pessah et al. 2006) with

those of mean field dynamos and large scale transport to fully model angular momentum transport in accretion disks.

6 Gauge Issues

A subtle aspect of the helicity density equations (21) and (22) is the issue of gauge non-invariance. In the absence of boundary flux terms or time dependent terms, the magnetic helicity is gauge invariant relative to an arbitrary choice of initial value. This is a straightforward consequence of Eq. (7). Since $\mathbf{E}\cdot\mathbf{B}$ is gauge invariant under any circumstance, the sum of the time dependent term on the left minus the divergence term on the right is always gauge invariant (even though the flux itself need not itself be gauge invariant). If the flux term vanishes, then the time derivative term is gauge invariant. If the time derivative term vanishes, then the leftover flux term is gauge invariant. This was used by Blackman and Field (2000b) to estimate an energy associated with the ejected magnetic helicity into coronae by a steady state dynamo. Mitra et al. (2010) show numerically that indeed the diffusive magnetic helicity fluxes that arise naturally across the mid plane in a system forced with oppositely signed kinetic helicities are gauge invariant. In the steady-state the divergence is invariant at every point so one can obtain the spatial dependence of the flux. These principles were also verified in Hubbard and Brandenburg (2010) and apply even to oscillatory dynamos by first identifying a gauge for which the helicity is steady (Del Sordo et al. 2013), which eliminates the dependent terms and the divergence term emerges as gauge invariant.

Additional subtleties of gauge invariance in the different context of shearing boxes are discussed in Candelaresi et al. (2011) and Hubbard and Brandenburg (2011).

Gauge non-invariance is closely related to the fact that for open boundaries, the amount of external field linkage is not in general specified. That is, the amount of field linkage inside the boundary can be the same for different amounts of exterior linkage. Fixing the gauge for the vector potential removes this ambiguity in that gauge. In actuality, one can choose a gauge, work in this gauge to study helicity dynamics, and then calculate physical quantities that are gauge invariant. The gauge non-invariance does not change the role of magnetic helicity as an intermediate conceptual tool.

However to interpret physically the magnetic helicity, gauge invariant versions can be helpful. Subramanian and Brandenburg (2006) developed a generalized local helicity density whose evolution reduces to the above Eqs. (21) and (22) in the absence of flux terms. In the presence of flux terms, their equation has the same form but with a different helicity density that is gauge invariant. For a turbulent system, with large scale separation between fluctuating and mean quantities, their gauge invariant helicity density associated with small scale quantities is similar to what is obtained for the usual magnetic helicity density in the Coulomb gauge because the gauge variant boundary terms become small in their averaging procedure. In the context of the Galaxy, Shukurov et al. (2006) solved the mean field induction equation for $\overline{\mathbf{B}}$ using this gauge invariant helicity density.

The gauge invariant relative magnetic helicity (Berger and Field 1984; Finn and Antonsen 1985; Bellan 2000) referred to earlier, was developed for more direct interpretations of observations originally in the solar context. This quantity involves separating global space into two parts, a region of physical interest and the exterior to this region. The relative magnetic helicity is specifically the difference between the magnetic helicity of the system integrated over global space minus that associated with an integral over global space where the field in region of physical interest is replaced by a vacuum, potential field, namely $H_R \equiv \int \mathbf{A}\cdot\mathbf{B}dV - \int \mathbf{A}_p\cdot\mathbf{B}_p dV$, where $\mathbf{B}_p = \nabla\times\mathbf{A}_p$ and $\mathbf{B}_p$ is the potential field. In this

way the external linkage is removed, and what remains is gauge invariant. The time evolution equation for H_R is then (Berger and Field 1984)

$$\partial_t H_R = -2c \int \mathbf{E} \cdot \mathbf{B} dV - \int \nabla \cdot (\mathbf{E} \times \mathbf{A}_p) dV. \tag{32}$$

All terms in this generalized relative magnetic helicity conservation equation are gauge invariant. Not only is the divergence term gauge invariant but the flux itself is gauge invariant. Démoulin and Berger (2003) have shown how the rate of injection of relative magnetic helicity into the solar corona depends on measurable quantities at the footprints of the anchoring fields. Sorting out the relation between the relative magnetic helicity, the current helicity, and the gauge variant magnetic helicity in theoretical calculations warrants further attention.

7 Summary and Conclusions

Tracking magnetic helicity in MHD systems is an important, unifying tool to understand the processes by which large scale magnetic fields form and evolve in both astrophysical and laboratory plasmas. The purpose of this review has been to provide one path through the forest as a conceptual primer to the literature. Three key principles underlie the role of magnetic helicity in all contexts: (1) magnetic helicity is a measure of twist, linkage or writhe; (2) magnetic helicity is better conserved than magnetic energy under most circumstances for a closed system with or without velocity flows; (3) the energy in a helical magnetic field is minimized when the field relaxes to the largest scale available consistent with the boundary conditions.

The importance of magnetic helicity for large scale field generation is evident from early studies of helical MHD turbulence (Pouquet et al. 1976), but incorporating its role into a 21st century dynamical mean field theory has emerged only in the pas decade or so. The 20th century textbook dynamos, unlike 21st century theory, do not conserve magnetic helicity and as such were unable to predict or reveal how LSDs saturate. A key aspect of 21st century theory is that the growth of large scale fields, facilitated by an EMF, involves growth of large scale magnetic helicity and small scale magnetic helicity of the opposite sign. In the absence of helicity fluxes, the small scale build up suppresses further growth of large scale field. In the case of sheared rotators, unless helicity fluxes can remove the offending small scale magnetic helicity, the large scale field not only saturates but may even decay. Alternatively expressed, it seems that astrophysical dynamos, like laboratory plasma dynamos may involve an EMF that is commonly aided or sustained by the divergence of small scale helicity fluxes. In a quasi-steady state for the sun, a crude minimalist prediction is that both signs of helical magnetic fields should appear in the northern hemisphere with small scale left handed structures and right handed large scale structures with the reversed combination in the southern hemisphere. More efforts to measure the spectral distribution of helical fields in the solar corona and wind would be valuable. Large scale dynamo models for the galaxy and for accretion disks that incorporate magnetic helicity dynamics have also been emerging.

Accretion disks pose an interestingly rich opportunity of study for helicity dynamics and large scale dynamos because traditionally large scale dynamo theory has been studied independent of theories of angular momentum transport. The ubiquity of large scale dynamos seen in simulations and the ubiquity of observed astrophysical coronae and jets indicates that a significant contribution to angular momentum transport comes from large scale fields.

This needs to be incorporated into a combined mean field accretion disk theory that captures local and large scale angular momentum transport, and large scale field growth.

Coronae of stars, disks, and laboratory plasmas are all magnetically energy dominated. In magnetically dominated environments the principles of magnetic helicity evolution have long been helpful to understand the evolution of magnetic structures subject to their foot-point motions. The helicity injection by foot-point motions is analogous to injection of small scale helicity in laboratory devices, where the system responds by relaxing the helicity to large scales In astrophysical coronae, it is likely that some contribution from both signs rather than a single sign are injected, so the relaxation process must take this into consideration globally, even if local structures are injected with primarily one sign. It was in fact in the context of laboratory plasma magnetic relaxation where the importance of helicity fluxes was first identified.

Finally, as reviewed herein, the basic properties of magnetic helicity also underlie its role in making large scale helical fields resilient to turbulent diffusion. Recent work on this topic for closed systems may strengthen the potential efficacy of fossil field origin of large scale fields in some astrophysical contexts. A helical field (in the absence of global helicity fluxes) is much more resilient to turbulent diffusion than non-helical large scale fields. The effect is best understood not as reduction of the turbulent diffusion coefficient, but rather as a competition between the unfettered turbulent diffusion and additional competing tendency for helicity to relax back toward the largest scales. The driver for this inverse transfer is the very small scale magnetic helicity that is sourced by initial diffusion from the large scale helicity in the first place.

Acknowledgements I acknowledge NSF grant AST-1109285, and thank the organizers of the ISSI Workshop on "Multi-Scale Structure Formation and Dynamics of Cosmic Plasmas", and the organizers of the Lyman Spitzer 100th birthday conference for engaging meetings in Bern and Princeton respectively. I also acknowledge particular discussions with P. Bhat, A. Bhattacharjee, A. Brandenburg, F. Ebrahimi, G. Field, A. Hubbard, F. Nauman, J. Stone and K. Subramanian.

References

K. Asada, M. Inoue, M. Nakamura, S. Kameno, H. Nagai, Astrophys. J. **682**, 798 (2008)
S.A. Balbus, Annu. Rev. Astron. Astrophys. **41**, 555 (2003)
S.A. Balbus, J.F. Hawley, Astrophys. J. **376**, 214 (1991)
S.A. Balbus, J.F. Hawley, Rev. Mod. Phys. **70**, 1 (1998)
R. Beck, Space Sci. Rev. **166**, 215 (2012)
P.M. Bellan, *Spheromaks* (Imperial College Press, London, 2000)
M.A. Berger, G.B. Field, J. Fluid Mech. **147**, 133 (1984)
P. Bhat, K. Subramanian, Mon. Not. R. Astron. Soc. **429**, 2469 (2013)
P. Bhat, E.G. Blackman, K. Subramanian, Mon. Not. R. Astron. Soc. **438**, 2954 (2014)
A. Bhattacharjee, E. Hameiri, Phys. Rev. Lett. **57**, 206 (1986)
E.G. Blackman, Recent developments in magnetic dynamo theory, in *Lecture Notes in Physics*, vol. 614, 2003, p. 432
E.G. Blackman, Plasma Phys. Control. Fusion **46**, 423 (2004)
E.G. Blackman, G.B. Field, Astrophys. J. Lett. **534**, 984 (2000a)
E.G. Blackman, G.B. Field, Mon. Not. R. Astron. Soc. **318**, 724 (2000b)
E.G. Blackman, G.B. Field, Phys. Rev. Lett. **89**, 265007 (2002)
E.G. Blackman, G.B. Field, Phys. Plasmas **11**, 3264 (2004)
E.G. Blackman, A. Brandenburg, Astrophys. J. **579**, 359 (2002)
E.G. Blackman, A. Brandenburg, Astrophys. J. Lett. **584**, L99 (2003)
E.G. Blackman, A. Hubbard, Mon. Not. R. Astron. Soc. (2014, drafted for submission)
E.G. Blackman, M.E. Pessah, Astrophys. J. **704**, L113 (2009)
E.G. Blackman, K. Subramanian, Mon. Not. R. Astron. Soc. **429**, 1398, BS13 (2013)

E.G. Blackman, A. Frank, C. Welch, Astrophys. J. **546**, 288 (2001)
R.D. Blandford, D.G. Payne, Mon. Not. R. Astron. Soc. **199**, 883 (1982)
J. Braithwaite, H.C. Spruit, Nature **431**, 819 (2004)
A. Brandenburg, in *Theory of Black Hole Accretion Disks*, ed. by M.A. Abramowicz, G. Bjornsson, J.E. Pringle (Cambridge University Press, Cambridge, 1998), p. 61
A. Brandenburg, Astrophys. J. **550**, 824 (2001)
A. Brandenburg, Astrophys. J. **625**, 539 (2005)
A. Brandenburg, Astrophys. J. **697**, 1206 (2009)
A. Brandenburg, K.J. Donner, Mon. Not. R. Astron. Soc. **288**, L29 (1997)
A. Brandenburg, A. Lazarian, Space Sci. Rev. **178**, 163 (2013)
A. Brandenburg, K. Subramanian, Phys. Rep. **417**, 1 (2005)
A. Brandenburg, A. Nordlund, R.F. Stein, U. Torkelsson, Astrophys. J. **446**, 741 (1995)
A. Brandenburg, D. Sokoloff, K. Subramanian, Space Sci. Rev. **169**, 123 (2012)
A. Brandenburg, K. Subramanian, A. Balogh, M.L. Goldstein, Astrophys. J. **734**, 9 (2011)
A. Brandenburg, D. Sokoloff, K. Subramanian, Space Sci. Rev. **169**, 123 (2012)
V. Bujarrabal, A. Castro-Carrizo, J. Alcolea, C. Sánchez Contreras, Astron Astrophys. **377**, 868 (2001)
S. Candelaresi, A. Hubbard, A. Brandenburg, D. Mitra, Phys. Plasmas **18**, 012903 (2011)
J. Chae, Y.-J. Moon, Y.-D. Park, Sol. Phys. **223**, 39 (2004)
L. Chamandy, K. Subramanian, A. Shukurov, Mon. Not. R. Astron. Soc. **428**, 3569 (2013)
P. Charbonneau, SASS **39** (2013)
C.J. Copi, F. Ferrer, T. Vachaspati, A. Achúcarro, Phys. Rev. Lett. **101**, 171302 (2008)
A. Díaz-Gil, J. García-Bellido, M. García Pérez, A. González-Arroyo, Phys. Rev. Lett. **100**, 241301 (2008)
S.W. Davis, J.M. Stone, M.E. Pessah, Astrophys. J. **713**, 52 (2010)
P. Démoulin, M.A. Berger, Sol. Phys. **215**, 203 (2003)
F. Del Sordo, G. Guerrero, A. Brandenburg, Mon. Not. R. Astron. Soc. **429**, 1686 (2013)
M. Dikpati, P.A. Gilman, Space Sci. Rev. **144**, 67 (2009)
F. Ebrahimi, A. Bhattacharjee, Phys. Rev. Lett. **112**, 125003 (2014)
G. Field, AIPC **144**, 324 (1986)
G.B. Field, E.G. Blackman, Astrophys. J. **572**, 685 (2002)
G.B. Field, S.M. Carroll, Phys. Rev. D, Part. Fields **62**, 103008 (2000)
G.B. Field, R.D. Rogers, Astrophys. J. **403**, 94 (1993)
J.M. Finn, T.M. Antonsen, Comments Plasma Phys. Control. Fusion **9**, 111123 (1985)
D.C. Gabuzda, D.M. Christodoulou, I. Contopoulos, D. Kazanas, Int. J. Mod. Phys. Conf. Ser. **355**, 012019 (2012)
D.C. Gabuzda, V.M. Vitrishchak, M. Mahmud, S.P. O'Sullivan, Mon. Not. R. Astron. Soc. **384**, 1003 (2008)
S.E. Gibson et al., Astrophys. J. **574**, 1021 (2002)
G.A. Glatzmaier, Annu. Rev. Earth Planet. Sci. **30**, 237 (2002)
O. Gressel, Mon. Not. R. Astron. Soc. **405**, 41 (2010)
A.V. Gruzinov, P.H. Diamond, Phys. Plasmas **3**, 1853 (1996)
X. Guan, C.F. Gammie, Astrophys. J. **728**, 130 (2011)
J. Hao, M. Zhang, Astrophys. J. **733**, L27 (2011)
T. Heinemann, J.C. McWilliams, A.A. Schekochihin, Phys. Rev. Lett. **107**, 255004 (2011)
A. Hubbard, A. Brandenburg, Geophys. Astrophys. Fluid Dyn. **104**, 577 (2010)
A. Hubbard, A. Brandenburg, Astrophys. J. **727**, 11 (2011)
H. Ji, S.C. Prager, Magnetohydrodynamics **38**, 191 (2002)
T. Kahniashvili, A.G. Tevzadze, A. Brandenburg, A. Neronov, Phys. Rev. D **87**, 083007 (2013)
A.P. Kazantsev, J. Exp. Theor. Phys. **26**, 1031 (1968)
P.J. Käpylä, M.J. Korpi, A. Brandenburg, Astron. Astrophys. **491**, 353 (2008)
P.J. Käpylä, M.J. Korpi, Mon. Not. R. Astron. Soc. **413**, 901 (2011)
K. Kemel, A. Brandenburg, H. Ji, Phys. Rev. E, Stat. Nonlinear Soft Matter Phys. **84**, 056407 (2011)
N.I. Kleeorin, A.A. Ruzmaikin, Magnetohydrodynamics **18**, 116 (1982)
F. Krause, K.H. Rädler, *Mean Field Magnetohydrodynamics and Dynamo Theory* (Pergamon, Elmsford, 1980)
A. Konigl, Astrophys. J. **342**, 208 (1989)
R.M. Kulsrud, E.G. Zweibel, Rep. Prog. Phys. **71**, 046901 (2008)
R.M. Kulsrud, R. Cen, J.P. Ostriker, D. Ryu, Astrophys. J. **480**, 481 (1997)
G. Lesur, G.I. Ogilvie, Astron. Astrophys. **488**, 451 (2008)
E.-K. Lim, H. Jeong, J. Chae, Y.-J. Moon, Astrophys. J. **656**, 1167 (2007)
R.V.E. Lovelace, D.M. Rothstein, G.S. Bisnovatyi-Kogan, Astrophys. J. **701**, 885 (2009)
D. Lynden-Bell, Mon. Not. R. Astron. Soc. **369**, 1167 (2006)
M. Lyutikov, V.I. Pariev, D.C. Gabuzda, Mon. Not. R. Astron. Soc. **360**, 869 (2005)

J. Maron, E.G. Blackman, Astrophys. J. **566**, L41 (2002)
S.F. Martin, A.H. McAllister, Geophys. Monogr. **99**, 127 (1997)
D. Mitra, A. Brandenburg, Mon. Not. R. Astron. Soc. **420**, 2170 (2012)
D. Mitra, S. Candelaresi, P. Chatterjee, R. Tavakol, A. Brandenburg, Astron. Nachr. **331**, 130 (2010)
H.K. Moffatt, *Magnetic Field Generation in Electrically Conducting Fluids* (Cambridge University Press, Cambridge, 1978)
S. Ortolani, D.D. Schnack, *Magnetohydrodynamics of Plasma Relaxation* (World Scientific, Singapore, 1993)
K. Park, E.G. Blackman, Mon. Not. R. Astron. Soc. **423**, 2120 (2012)
E.N. Parker, Clarendon/Oxford University Press, Oxford/New York, 1979, 858 pp.
R.F. Penna, R. Narayan, A. Sądowski, Mon. Not. R. Astron. Soc. **436**, 3741 (2013)
M.E. Pessah, C.-K. Chan, D. Psaltis, Phys. Rev. Lett. **97**, 221103 (2006)
A.A. Pevtsov, R.C. Canfield, T. Sakurai, M. Hagino, Astrophys. J. **677**, 719 (2008)
A. Pouquet, U. Frisch, J. Leorat, J. Fluid Mech. **77**, 321 (1976)
H. Ji, S.C. Prager, J.S. Sarff, Phys. Rev. Lett. **74**, 2945 (1995)
R.E. Pudritz, M.J. Hardcastle, D.C. Gabuzda, Space Sci. Rev. **169**, 27 (2012)
P.H. Roberts, E.M. King, Rev. Plasma Phys. **76**, 096801 (2013)
G. Rüdiger, L.L. Kichatinov, Astron. Astrophys. **269**, 581 (1993)
D.M. Rust, Geophys. Monogr. **111**, 221 (1999)
D.M. Rust, A. Kumar, Astrophys. J. **464**, L199 (1996)
A.A. Ruzmaikin, D.D. Sokolov, A.M. Shukurov (eds.), *Magnetic Fields of Galaxies* (Kluwer Academic, Dordrecht, 1988)
A. Shukurov, Lect. Notes Phys. **664**, 113 (2005)
A. Shukurov, D. Sokoloff, K. Subramanian, A. Brandenburg, Astron. Astrophys. **448**, L33 (2006)
A.A. Schekochihin, S.C. Cowley, G.W. Hammett, J.L. Maron, J.C. McWilliams, New J. Phys. **4**, 84 (2002)
C.J. Schrijver, C. Zwaan, *Solar and Stellar Magnetic Activity* (Cambridge University Press, Cambridge, 2000)
P.W. Schuck, Astrophys. J. **632**, L53 (2005)
V.B. Semikoz, D.D. Sokoloff, J.W.F. Valle, J. Cosmol. Astropart. Phys. **6**, 8 (2012)
J.B. Simon, J.F. Hawley, K. Beckwith, Astrophys. J. **730**, 94 (2011)
K.A. Sorathia, C.S. Reynolds, J.M. Stone, K. Beckwith, Astrophys. J. **749**, 189 (2012)
S. Sridhar, N.K. Singh, ArXiv e-prints (2013)
H.R. Strauss, Phys. Fluids **28**, 2786 (1985)
H.R. Strauss, Phys. Fluids **29**, 3008 (1986)
K. Subramanian, Phys. Rev. Lett. **90**, 245003 (2003)
K. Subramanian, Astron. Nachr. **331**, 110 (2010)
K. Subramanian, A. Brandenburg, Astrophys. J. Lett. **648**, L71 (2006)
S. Sur, A. Shukurov, K. Subramanian, Mon. Not. R. Astron. Soc. **377**, 874 (2007)
T.K. Suzuki, S.-i. Inutsuka, arXiv:1309.6916 (2013)
J.B. Taylor, Phys. Rev. Lett. **33**, 1139 (1974)
J.B. Taylor, Rev. Mod. Phys. **58**, 741 (1986)
A.G. Tevzadze, L. Kisslinger, A. Brandenburg, T. Kahniashvili, Astrophys. J. **759**, 54 (2012)
S.M. Tobias, F. Cattaneo, N.H. Brummell, Astrophys. J. **685**, 596 (2008)
C.L. Van Eck et al., Astrophys. J. **728**, 97 (2011)
E.T. Vishniac, Astrophys. J. **696**, 1021 (2009)
E.T. Vishniac, A. Brandenburg, Astrophys. J. **475**, 263 (1997)
E.T. Vishniac, J. Cho, Astrophys. J. **550**, 752 (2001)
E.T. Vishniac, D. Shapovalov, Astrophys. J. **780**, 144 (2014)
Y.-M. Wang, N.R. Sheeley Jr., Astrophys. J. **599**, 1404 (2003)
L.M. Widrow, D. Ryu, D.R.G. Schleicher, K. Subramanian, C.G. Tsagas, R.A. Treumann, Space Sci. Rev. **166**, 37 (2012)
L. Woltjer, Proc. Natl. Acad. Sci. USA **44**, 489 (1958a)
L. Woltjer, Proc. Natl. Acad. Sci. USA **44**, 833 (1958b)
T.A. Yousef, A. Brandenburg, G. Rüdiger, Astron. Astrophys. **411**, 321 (2003)
T.A. Yousef, T. Heinemann, A.A. Schekochihin, N. Kleeorin, I. Rogachevskii, A.B. Iskakov, S.C. Cowley, J.C. McWilliams, Ph R L **100**, 184501 (2008)
H. Zhang, S. Yang, Y. Gao, J. Su, D.D. Sokoloff, K. Kuzanyan, Astrophys. J. **719**, 1955 (2010)
H. Zhang, D. Moss, N. Kleeorin, K. Kuzanyan, I. Rogachevskii, D. Sokoloff, Y. Gao, H. Xu, Astrophys. J. **751**, 47 (2012)